Summer 2019

The Study of Flow Hydrodynamics and Transport Processes Over Mixed Bedrock-Alluvial Reaches

Mohammad Sadegh Jafarinik

THE STUDY OF FLOW HYDRODYNAMICS AND TRANSPORT PROCESSES OVER MIXED BEDROCK-ALLUVIAL REACHES

by

Mohammad Sadegh Jafarinik

Bachelor of Science
Shahid Beheshti University

Master of Science
Amirkabir University

Submitted in Partial Fulfillment of the Requirements

For the Degree of Doctor of Philosophy in

Civil Engineering

College of Engineering and Computing

University of South Carolina

2019

Accepted by:

Enrica Viparelli, Major Professor

Hanif Chaudhry, Committee Member

Jasim Imran, Committee Member

Michal Tal, Committee Member

Cheryl L. Addy, Vice Provost and Dean of the Graduate School

ACKNOWLEDGEMENTS

The author thanks the USC geotechnical engineering group for providing access to the equipment to perform sieve analyses. This research was supported by the United States National Science Foundation through award EAR 1250641 and by the University of South Carolina through Dr. Enrica Viparelli's start up fund. The experimental dataset has been made publicly available through the assistance of the Sediment Experimentalist Network (SEN) (NSF 1324660).

ABSTRACT

Research efforts on mixed bedrock-alluvial rivers primary focused on the bedrock incision and very few studies investigated the alluvial morphodynamics of such systems. To the best of my knowledge none of these models have been considered the spatial variability of the sediment grain size of the bed surface in mixed bedrock-alluvial reaches and very few models focused on the spatial changes in alluvial cover within these reaches. Furthermore, a perusal of the literature on mixed bedrock-alluvial river morphodynamics reveals that very little information is available on 1) bedform geometry and flow resistances and 2) sediment sorting patterns in presence of a non-erodible bedrock surface. Understanding the interactions between flow and sediment transport processes in mixed bedrock-alluvial reaches is important to e.g. predict the long-term river response to engineering works, changes in climate and sediment supply; perform large scale sediment budgets; and determine the quality of the riparian habitat. I thus designed and performed laboratory experiments to investigate the effects of a model bedrock surface on flow hydraulics and sediment transport processes. I derived a novel mathematical formulation of mixed bedrock-alluvial morphodynamics that accounts for the non-uniformity of the bed material. I implemented this formulation in a one- dimensional model of river morphodynamics. The experiments revealed that equilibrium in mixed bedrock-alluvial reaches is characterized by flow acceleration in the streamwise direction when the slope of the bedrock surface is milder than the equilibrium slope of an alluvial reach transporting the

same discharge and sediment load. The morphodynamic response to this spatial flow acceleration is characterized by 1) streamwise reduction in the alluvial cover, 2) streamwise reduction in bedform height, and 3) formation of a pattern of downstream fining of the bed surface sediment. The morphodynamic model was validated at laboratory scale against the experimental results. The validated model was then used to study the changes in flow hydraulics and sediment transport processes in mixed bedrock-alluvial reaches with a bedrock surface slope that was steeper than the alluvial equilibrium slope of a channel subjected to the same discharge and sediment supply of the mixed bedrock-alluvial reach of interest. The numerical results at equilibrium show that in this case flow velocity decreased on the mixed bedrock-alluvial reach in streamwise direction. The morphodynamic effects of this spatial flow deceleration were 1) a streamwise increase in alluvial cover, and 2) the formation of a pattern of downstream coarsening of the bed surface sediment. The morphodynamic formulation presented in this dissertation will be applied at field scale on the gravel bed Buech River, Southeastern France, to study the impacts of dam construction and gravel mining on a mixed bedrock-alluvial gravel bed river, and to identify possible restoration strategies to control the observed widespread erosion and the associated deterioration of the aquatic and riparian habitat.

TABLE OF CONTENTS

ACKNOWLEDGEMENTS iii

ABSTRACT iv

LIST OF TABLES viii

LIST OF FIGURES ix

LIST OF SYMBOLS x

CHAPTER 1: INTRODUCTION 1

CHAPTER 2: ALLUVIAL MORPHODYNAMICS OF MIXED BEDROCK-ALLUVIAL REACHES TRANSPORTING MIXED-SIZE SAND. LABORATORY EXPERIMENT 5

2.1 Introduction 5

2.2 Background information on 1D models of alluvial morphodynamics relevant to the present study 8

2.3 Overview on the experiments 13

2.4 Results 17

2.5 Discussion 26

2.6 Conclusion 36

CHAPTER 3: MORPHODYNAMIC MODEL OF MIXED BEDROCK-ALLUVIAL REACHES CARRYING NON-UNIFORM BED MATERIAL 52

3.1 Introduction 52

3.2 Model formulation 55

3.3 Empirical relations to validate the model at laboratory scale 66

3.4 Model validation at laboratory scale 75

3.5 Discussion 80

3.6 Conclusion 82

CHAPTER 4: CONCLUSION 93

REFERENCES 99

APPENDIX A: PROCEDURES TO REMOVE SIDEWALL EFFECTS AND EINSTEIN DECOMPOSITION 108

LIST OF TABLES

Table 2.1 Experimental conditions 39

Table 2.2 Average water surface elevation and standard deviation of the water surface elevation for different measurement durations in Run 5 at 5 m from the test reach entrance 40

LIST OF FIGURES

Figure 2.1 Schematic picture of the long profile of the flume.....41

Figure 2.2 Grain size distribution of the bedload material 42

Figure 2.3 Time series of bed elevation fluctuation 43

Figure 2.4 Results of fully alluvial Runs 44

Figure 2.5 Time series of bed elevation fluctuation for Run 3 45

Figure 2.6 Results for mixed bedrock-alluvial 46

Figure 2.7 Alluvial cover fraction.....47

Figure 2.8 Friction coefficient and nondimensional bed shear stresses 48

Figure 2.9 *Ashida and Michiue* (1972) formulation 49

Figure 2.10 Grain size distribution of the surface.....50

Figure 2.11 *Vanoni* (1974) diagram.....51

Figure 3.1 Schematic picture of the modeled domain 85

Figure 3.2 Alluvial cover fraction formulation of *Viparelli et al.* (2015).....86

Figure 3.3 Flow resistances analysis of the experimental data.....87

Figure 3.4 Numerical results for fully alluvial Runs 88

Figure 3.5 Numerical results for mixed bedrock-alluvial Runs.....89

Figure 3.6 Grain size distributions of the surface material.....90

Figure 3.7 schematic plot of the bedrock-alluvial transition 91

Figure 3.8 Numerical results for Bedrock-alluvial transition.....92

LIST OF SYMBOLS

A_b	Area of the bed region
A_{cs}	Cross sectional area
A_w	Area of the wall region
C_f	Friction coefficient
$C_{f,b}$	Friction coefficient of bed region
$C_{f,ba}$	Friction coefficient associated with alluvium
$C_{f,bas}$	Friction coefficient of alluvial cover associated with skin friction
$C_{f,bb}$	Friction coefficient associated with bedrock
$C_{f,cs}$	Friction coefficient of cross section
$C_{f,w}$	Friction coefficient of wall region
C_{fb}	Side wall corrected friction coefficient
D_g	Geometric mean diameter of the sediment supply
D_i	Grain size diameter
D_{sg}	Geometric mean diameter of the surface material
F_i	Volume fraction content of sediment for generic grain sizes
Fr	Froude number
f_w	Friction factor of wall region
g	Acceleration of gravity
H	Water depth

H_o Equilibrium water depth

K_{sb} Roughness height of the bedrock

L_{ac} Minimum thickness of alluvial cover

P_b wetted perimeter of bed region

P_c Alluvial cover fraction

P_{cs} wetted perimeter of cross section

P_w Wetted perimeter of wall region

q^*_{bsi} Nondimensional bedload transport rate per unit width for a generic grain size

q_b Bedload transport rate per unit channel width

q_{bi} Bedload transport rate per unit width for generic grain sizes

q_{bm} Volumetric bed material load per unit channel width

q_{bT} Total bedload transport rate per unit width

q_c Sediment transport capacity

R Submerged specific gravity

r_b Hydraulic radius of bed region

r_{cs} Hydraulic radius of cross section

Re_b Reynolds number of bed region

Re_{cs} Reynolds number of cross section

Re_w Reynolds number of wall region

$R_{h,b}$ Hydraulic radius of ideal flow over bedrock surface

r_w Hydraulic radius of wall region

S_b Bedrock slope

S_f Friction slope

S_o Equilibrium bed slope

U Averaged flow velocity

η_a Average elevation of alluvial deposit

η_b Bedrock elevation

η_{bd} Bedrock elevation at the downstream

λ_p Bed material porosity

ξ_d Water surface elevation

ρ Water density

σ_g Standard deviation of the sediment supply

σ_n Standard deviation of the bed elevation

τ^* Nondimensional shear stress

τ^*_{bas} Nondimensional shear stress of alluvial cover associated with skin friction

τ^*_{bsi} Nondimensional shear stress associated with skin friction for a generic grain size

τ^*_{refi} Reference shields number for generic grain sizes

τ^*_{scg} Grain size nonspecific reference value for shields number

τ_b Bed shear stress

τ_{bas} Shear stress of alluvial cover associated with skin friction

CHAPTER 1

INTRODUCTION

This study investigates the flow characteristics and sediment transport processes in mixed bedrock-alluvial reaches transporting non-uniform sediment. Here I defined mixed bedrock-alluvial reaches those with more than 5% of the channel bed composed of exposed bedrock and with the rest of the channel bed covered by a relatively thin layer of alluvium [Howard, 1998]. Mixed bedrock-alluvial reaches have been frequently observed in upland areas where the bed material is relatively coarse, is preferentially transported as bedload, and small scale bedforms such as dunes are generally absent [e.g. Whipple et al., 2000; Whipple and Tucker, 2002; Whipple, 2004; Sklar and Dietrich, 2004; Turowski et al., 2007; Gasparini et al., 2007; Chatanantavet and Parker, 2008, 2009; Lamb et al., 2008; Lague, 2010, 2014; Hodge et al., 2011, 2016; Chatanantavet et al., 2013; Johnson, 2014; Zhang et al., 2014; Inoue et al., 2014]. Recent field studies demonstrated that mixed bedrock-alluvial rivers can also be found in lowland areas, where the bed material is relatively fine, and small scale bedforms are present.

Nittrouer et al. [2011] and Shaw et al. [2013] documented the presence of dune fields in the mixed bedrock-alluvial reaches of the Mississippi River and of the Wax Lake Delta distributary channels. Carling et al. [2000a, b] described isolated dunes in the German Rhine River that migrate on top of an immobile layer of coarse gravel. Tuijnder et

al. [2009] performed laboratory experiments on the equilibrium characteristics of supply limited dunes on an immobile gravel layer under steady and uniform hydraulic conditions and found that the dune height and wavelength increased with the average thickness of the layer overlying the gravel substratum. These studies, however, do not present any quantitative estimate of the difference between flow resistances in a fully alluvial and in a mixed bedrock-alluvial reach with the same formative flow and bed material supply. In particular, there is a lack of information on how flow resistances associated with bedforms (form drag) and with bed material grain size (skin friction) differs in alluvial and mixed bedrock-alluvial reaches. Form drag predictors available in the literature [e.g. Engelund and Hansen, 1967; Chaubert and Chauvin, 1963; Wright and Parker, 2004] were mostly determined for fully alluvial systems. Quantitative information on bedform geometry and sediment sorting patterns in mixed bedrock-alluvial reaches is necessary to adequately characterize the alluvial morphodynamics, which is important for habitat preservation, restoration projects and the performance of sediment budgets [Viparelli et al., 2013 and 2015].

Numerical models of mixed bedrock-alluvial river morphodynamics have generally focused on bedrock incision and the alluvial morphodynamics of these river reaches has been long overlooked. Only few, recent studies have considered the alluvial morphodynamics of such systems [Zhang et al., 2014; Viparelli et al., 2015]. Viparelli et al. [2015] developed a morphodynamic model that can track the transition from an alluvial to a mixed bedrock-alluvial reach and vice versa and showed that at equilibrium the flow cannot be uniform on the mixed bedrock-alluvial reaches. In other words, at equilibrium flow characteristics in a mixed bedrock-alluvial reaches do not change in time but change

in space. To the best of my knowledge, the alluvial morphodynamics of mixed bedrock-alluvial reaches transporting nonuniform material and the equilibrium sorting patterns remain poorly studied problems with relevant real works applications. For example, understanding the spatial changes of the bed surface sediment in mixed bedrock-alluvial rivers is quite necessary to predict the responses to restoration projects.

Numerous empirical relations have been developed to predict sediment fluxes in alluvial rivers [see Garcia, 2008 for a thorough review]. Some relations considered uniform material, others explicitly accounted for the nonuniformity of the bed material. Very few studies, however, tested these equations in mixed bedrock-alluvial reaches where the bedrock directly interferes with the in-channel transport processes. Thus, research is needed to quantify sediment transport processes in mixed bedrock-alluvial systems.

Here I presented the results of laboratory experiments specifically designed to 1) understand how equilibrium flow characteristics, bedform geometry and bed surface material spatially change in mixed bedrock-alluvial rivers, and 2) determine if empirical relations for computing bedload transport in alluvial systems can be reasonably used to model bedload transport in "relatively mild" mixed bedrock-alluvial reaches. A novel mathematical formulation describing the alluvial morphodynamics of mixed bedrock-alluvial rivers transporting non-uniform bed material was derived and implemented in a one-dimensional (laterally-averaged) morphodynamic model. This model was validated against the laboratory data and used to investigate the characteristics of "relatively steep" mixed bedrock-alluvial reaches.

This manuscript is organized as follows: in chapter 2, I presented the experimental work and the analysis of the results. In chapter 3, I presented the mathematical formulation for the alluvial morphodynamics of mixed bedrock-alluvial rivers transporting non-uniform sediment, its validation at laboratory scale in a “relatively mild” flume, and the application to “relatively steep” mixed bedrock-alluvial reaches. I then discussed the results. The general conclusions and the future work are briefly discussed in Chapter 4.

CHAPTER 2

ALLUVIAL MORPHODYNAMICS OF MIXED BEDROCK-ALLUVIAL REACHES TRANSPORTING MIXED-SIZE SAND. LABORATORY EXPERIMENT

2.1 Introduction

Studies on the morphodynamics of bedrock and mixed bedrock-alluvial rivers have primarily focused on bedrock incision (e.g. Whipple et al., 2000; Whipple and Tucker, 2002; Whipple, 2004; Sklar and Dietrich, 2004; Turowski et al., 2007; Gasparini et al., 2007; Chatanantavet and Parker, 2008, 2009; Lamb et al., 2008; Lague, 2010, 2014; Hodge et al., 2011, 2016; Chatanantavet et al., 2013; Johnson, 2014; Inoue et al., 2014; Zhang et al., 2015), while the alluvial morphodynamics of mixed bedrock-alluvial rivers, which is important for e.g. habitat preservation, restoration projects and the performance of sediment budgets, has been long overlooked (Johnson and Whipple, 2007 and 2010; Finnegan et al. 2007, Viparelli et al., 2015). Due to the paucity of field and laboratory data and the lack of understanding of the interactions between sediment transport processes and the underlying hardily erodible surface (Carling et al. 2002a, b), there is a paucity of predictive models to estimate flow resistances and sediment fluxes in mixed bedrock-alluvial rivers. Very limited quantitative information is also available to account for the non-uniformity of the sediment size distribution in presence of a hardily erodible surface (Hodge et al., 2011, 2016).

Nittrouer et al. (2011) and Shaw et al. (2013) documented the presence of dune fields in the mixed bedrock-alluvial reaches of the Mississippi River and of the Wax Lake Delta distributary channels. Carling et al. (2000a, b) described isolated dunes in the German Rhine River migrating on top of an immobile layer of coarse gravel and noticed that the presence of dunes had an impact on the flow resistances. Tuijnder et al. (2009) performed laboratory experiments on the equilibrium characteristics of supply limited dunes on an immobile gravel layer and found that dune height and wavelength increased with the average thickness of the layer overlying the gravel substratum. These studies, however, did not propose predictive models to estimate flow resistances and bedform characteristics in reaches characterized by the interaction between a hardily erodible layer (bedrock or gravel) and the sediment transport.

Johnson (2014) noticed that to compute flow resistances in mixed bedrock-alluvial rivers transporting gravel as bed material the different roughness between the areas covered with alluvium and areas with exposed bedrock should be accounted for. He thus introduced an *equivalent friction coefficient* defined as the average friction coefficient of the alluvial and the bedrock patches (Johnson, 2014). To extend Johnson's model to rivers with relatively mild slopes and bed material in the range of pea gravel and sand the presence of bedforms such as dunes must be accounted for (Van Rijn, 1984).

Zhang et al. (2015) presented the first model of alluvial morphodynamics of mixed bedrock-alluvial rivers known to the authors that accounts for the coevolution of alluvial and incisional processes. The key difference between the Zhang et al. (2015) formulation and previous models of mixed bedrock-alluvial river morphodynamics is in the calculation of the alluvial cover, i.e., the average aerial fraction of the channel bed covered with

alluvium, which controls bedrock incision and alluvial processes (Sklar and Dietrich, 2004). In particular, Zhang et al. (2015) expressed the alluvial cover as a function of the geometric characteristics of the bedrock surface and not as the ratio between sediment supply rate and sediment transport capacity (Sklar and Dietrich, 2004).

Viparelli et al. (2015) modified the Zhang et al. (2015) formulation to study the impacts of land-building engineered diversions on the lowermost Mississippi River, which is a sand bed river with exposed bedrock and dune fields in the alluvial portion of the channel bed (e.g. Nittrouer et al. 2011). In particular, Viparelli et al. (2015) defined a minimum thickness of alluvial cover for complete alluviation of the channel bed based on dune height during floods. In this way they accounted for the geometric characteristics of the dune fields, which were hypothesized to have a significant influence on sand load calculations. Due to the lack of information on the influence of the bedrock surface on dune geometry, however, Viparelli et al. (2015) used a formulation to partition the flow resistances between skin friction and form drag in fully alluvial rivers (Wright and Parker, 2004). This formulation should have probably been modified to account for 1) the interactions between the hardily erodible bedrock surface and the migrating bedforms in the form drag calculations, and 2) the flow resistances associated with exposed bedrock (Johnson, 2014).

Here I presented the results of laboratory experiments specifically designed to study the interaction between a non-erodible surface (the model bedrock) and sediment transport processes in terms of 1) bedform geometry, 2) longitudinal sediment sorting patterns and 3) flow resistances. The experiments were performed in a sediment feed flume and the analysis focused on equilibrium conditions, i.e., conditions in which the elevation of the

alluvium averaged over a series of bedforms did not change in time (Anderson et al., 1975). Due to the limited length of the experimental facility, the experiments considered the case of bedload transport. In other words, the interaction between the suspended bed material load and the bedrock surface was not the scope of the present study.

This chapter is organized as follows, I first reported background information on one-dimensional morphodynamics models of alluvial and mixed bedrock-alluvial rivers that are relevant to this study. I then described the laboratory experiments and the relevant results. The spatial changes in flow resistances, bedload transport rates, grain size distribution of bed surface sediment and bedform geometry are discussed and interpreted using models, procedures and approaches developed to study the morphodynamics of fully alluvial rivers. This exercise shows that methods and procedures developed for fully alluvial rivers can be used to model the alluvial morphodynamics of mixed bedrock-alluvial systems if the presence of a non-erodible surface is explicitly accounted for in the calculations.

2.2 Background information on 1D models of alluvial morphodynamics relevant to the present study

Here I considered the case of a low slope river transporting sand and/or pea gravel, i.e. a system in which small scale bedforms such as dunes are likely present. The problem is simplified with assumptions and approximations that are at the base of most one-dimensional models of river morphodynamics. Some of these assumptions can be easily relaxed for site specific applications (e.g. Viparelli et al., 2011, 2015).

The river reach is modeled as a sediment feed flume analog, i.e. water and sediment are fed from upstream at a specified rate and streamwise changes in flow discharge and sediment supply are not considered (Blom et al., 2016). The channel has a rectangular cross section of constant width. The exchange of sediment between the river channel and the floodplain is not accounted for. The slope of the bedrock surface, S_b, is assumed to be constant in space and time. I also assumed

1) absence of subsidence, uplift and sea level changes,

2) uniform bed material,

3) no abrasion of gravel particles, and

4) equal friction coefficient for the alluvial and the bedrock areas.

In other words, due to the lack of predictive models linking bedform geometry and grain size distribution of the bed surface sediment with the presence of a non-erodible substrate, I did not consider the changes in roughness from fully alluvial to mixed bedrock-alluvial reaches. The experiments presented hereinafter provide novel and quantitative insight on how to relax assumptions (2) and (4).

Let's consider a sediment feed flume with a model bedrock reach and no alluvial cover (Figure 2.1a). The elevation of the downstream water surface base level is ξ_d and the elevation of the bedrock surface is denoted with η_b. When water and sediment supply are turned on, an alluvial deposit with a downstream migrating front forms (Figure 2.1b). The front eventually reaches the downstream end of the flume and, after sufficiently long time has elapsed, the system reaches a condition of equilibrium in which the average

elevation of the alluvial deposit, η_a, the slope of the alluvial reach and the water depth remain constant over time scales that are long compared to the time scales associated with bedform migration (Figure 2.1c) (Anderson et al., 1975; Parker, 2004).

Alluvial equilibrium

In alluvial rivers, the spatial and temporal evolution of an alluvial deposit is modeled with the Exner equation of conservation of bed material that, in a one-dimensional problem such as the experimental flume considered herein, takes the form

$$\left(1-\lambda_p\right)\frac{\partial \eta_a}{\partial t} = -\frac{\partial q_{bm}}{\partial x} \tag{2-1}$$

where λ_p denotes the bed porosity, t and x respectively are temporal and streamwise coordinates, and q_{bm} represents the volumetric bed material load per unit channel width, which is equal to the bed material transport capacity of the flow. It is important to note that q_{bm} represents temporal average over time scales that are long compared to the time scales characterizing bedform migration and bed material transport (Anderson et al., 1975). At equilibrium, the time rate of change of the deposit elevation η_a is equal to zero. Thus, the bed material load is equal to the bed material transport capacity and to the bed material feed rate (equation 2-1).

The bed material transport capacity is generally computed with empirical relations linking q_{bm} to the Shields number τ^*, i.e., the non-dimensional bed shear stress defined as $\tau_b/\rho RgD$, with τ_b denoting the bed shear stress, D the characteristic grain size of the bed material, ρ the water density and R the submerged specific gravity of the bed material

(Garcia, 2008). In particular, the bed material transport capacity is modeled with increasing functions of τ^* (Garcia, 2008). Recalling that at equilibrium q_{bm} does not change in space and time, the equilibrium bed shear stress τ_b has to be constant in the streamwise direction and in time. In other words, at alluvial equilibrium the flow can be modeled as steady and uniform over time scales that are long compared to the time scales of bedform migration (Anderson et al., 1975; Parker, 2004).

Equilibrium with a stable alluvial-bedrock transition

When the vertical distance between the downstream water surface base level and the bedrock is sufficiently small, the river reaches equilibrium conditions with exposed bedrock and steady but non-uniform flow (Viparelli et al., 2015). By defining a minimum thickness of alluvial cover for complete alluviation of the channel bed, L_{ac}, such that $\eta_b + L_{ac}$ represents the minimum elevation of the alluvial deposit for complete alluviation of the channel bed, when $\eta_a > \eta_b + L_{ac}$, the reach is defined to be alluvial. When $\eta_a < \eta_b + L_{ac}$ the reach is defined to be bedrock. In this formulation, an alluvial-bedrock or a bedrock-alluvial transition occurs when $\eta_a = \eta_b + L_{ac}$ (Figure 2.1d).

If the downstream water surface base level, ξ_d, is greater than the sum of the alluvial equilibrium flow depth $H_{o,}$ L_{ac} and η_{bd}, with η_{bd} denoting the elevation of the bedrock surface at the downstream end of the flume, conditions of alluvial equilibrium can be obtained. When $\xi_d < H_o + L_{ac} + \eta_{bd}$ exposed bedrock may characterize the equilibrium configuration of the model reach. In particular, if the slope of the bedrock surface S_b is smaller than the slope of an alluvial equilibrium reach subject to the same flow rate and

sediment supply of the bedrock reach, S_o, a stable alluvial-bedrock transition forms as illustrated in Figure 2.1d (Viparelli et al., 2015).

In the alluvial reach of Figure 2.1d the equilibrium bed slope is equal to S_o, the equilibrium flow depth is equal to H_o and the equilibrium bed material load is equal to the bed material transport capacity and to the feed rate. In the bedrock reach of Figure 2.1d, the limited vertical distance between the downstream water surface base level and the bedrock surface forces the equilibrium flow depth to decrease in the streamwise direction, i.e., downstream of a stable alluvial-bedrock transition the flow accelerates in space (Viparelli et al., 2015).

Recalling that the bed shear stress $\tau_b = \rho C_f U^2$, with C_f denoting a non-dimensional friction coefficient and U the mean flow velocity (Parker, 2004), if C_f is assumed to be the same in the alluvial and in the mixed bedrock-alluvial reaches (assumption 4), and U increases in the flow direction, the bed shear stress and the bed material transport capacity also increase in the streamwise direction. At equilibrium, however, the bed material load must be equal to the feed rate to satisfy sediment mass balance, and thus the bed material load in the mixed bedrock-alluvial reach should be smaller than the transport capacity.

The bed material load in mixed bedrock-alluvial reaches is generally modeled as the product of the bed material transport capacity q_c and the alluvial cover p_c, i.e., $q_{bm} = p_c q_c$ (Sklar and Dietrich, 2004; Zhang et al., 2015). Thus, if the friction coefficient C_f is assumed to be same in alluvial and mixed bedrock-alluvial reaches, the streamwise increasing bed material transport capacity downstream of a stable alluvial-bedrock transition should be balanced by p_c decreasing in the flow direction (Viparelli et al., 2015).

In other words, models of alluvial morphodynamics predict that downstream of a stable alluvial-bedrock transition the fraction of the channel bed covered with alluvium decreases in the flow direction, unless spatial changes in C_f are accounted for in the calculations.

Subsidence, uplift and changes in downstream water surface base level (assumption 1) result in a change in distance between the downstream water surface base level and the bedrock surface. If this distance increases (subsidence and base level rise), the alluvial-bedrock transition will migrate downstream. Conversely, it is reasonable to expect an upstream migration of the alluvial-bedrock transition in the case of base level fall and uplift.

2.3 Overview on the experiments

I performed the experiments in the 13 m long, 0.50 m wide and 0.9 m deep horizontal sediment feed flume in the Hydraulics Laboratory of Civil and Environmental Engineering Department at the University of South Carolina. A 6 m long and 0.19 m wide test reach was built with marine plywood to perform experiments on bedload transport. The entire flume length could not be used because the downstream most possible location for the sediment trap was at 8.5 m from the flume entrance. The cross section in the upstream part of the flume was gradually narrowed from 0.5 m to 0.19 m to reduce the likelihood of having three-dimensional bedforms and to limit the volume of sediment used in the experiments. This gradual reduction of the cross section occupied the first 2.5 m of the flume, leaving a 6 m long test reach.

The downstream water surface elevation was controlled with a tailgate. The constant flow rate was supplied from the head tank of the laboratory and measured with a

calibrated orifice plate. The model bedrock surface was a horizontal ($S_b = 0$) sheet of white plywood glued on to the bottom of the flume. Details on the experimental facility are available through the wiki page of the Sediment Experimentalists Network at http://sedexp.net/content/university-south-carolina-columbia-hydraulics-laboratory.

The experiments were performed with two types of sand: uniform sand with geometric mean diameter D_g = 1.11 mm and geometric standard deviation σ_g = 1.44, and non-uniform sand with D_g = 0.87 mm, and σ_g = 1.69. The grain size distribution of the sand used in the experiments is presented in Figure 2.2, where the grey line represents the size distribution of the uniform sand and the black line is the size distribution of the non-uniform sand. These materials were chosen to prevent suspended sediment transport and the formation of small-scale ripples.

I designed four groups of paired experimental runs (Run 1-8) summarized in Table 2.1 in terms of flow and sediment feed rates, downstream water surface elevation and sand type. Each pair of runs had the same flow rate, feed rate and sediment type, but differed for the downstream water surface base level, which dictated if mobile bed equilibrium was either fully alluvial or had a stable alluvial-bedrock transition. In the last column of Table 2.1 I reported whether the equilibrium was fully alluvial or had exposed bedrock.

The initial conditions of the experimental runs varied from one run to the other. The fully alluvial runs commenced with no alluvial deposit (Figure 2.1a). The runs with an equilibrium bedrock reach commenced with the alluvial equilibrium deposit obtained for the same flow and sediment feed rates (Figure 2.1c). The downstream water surface base level was gradually lowered to obtain a stable alluvial-bedrock transition at approximately

2 m from the flume entrance (Figure 2.1d), as further discussed in the result section. Noting that equilibrium conditions in a sediment feed flume are not dependent on the initial conditions, the initial conditions of the experimental runs did not influence the results presented below (Parker and Wilcock, 1993).

2.3.1 Experimental procedure

During each run, 20-minute long series of water surface elevation measurements were periodically recorded with Baumer sonar probes at 0.2 m, 1.9 m, 3.9 m and 5.95 m from the test reach entrance. The average water surface elevation was then calculated at each location. When the percent error between two consecutive water surface elevation measurements at the same location became smaller than 5%, I assumed that the system reached conditions of equilibrium.

At equilibrium, 20-minute long series of water surface elevation measurements were recorded at eight locations, i.e., 0 m, 0.3 m, 1 m, 2 m, 3 m, 4 m, 5 m and 6 m from the test reach entrance, and 30-minute long series of bed elevation measurements were recorded with a JSR ultrasonic sonar pulser (Wong et al., 2007) at 16 locations, i.e., 0.21 m, 0.51 m, 0.81 m, 1.21 m, 1.51 m, 1.81 m, 2.21 m, 2.51 m, 2.81 m, 3.21 m, 3.51 m, 3.81 m, 4.81 m, 5.21 m, 5.51 m and 5.81 m from the test reach entrance, to determine the average bed elevation, characterize bedform geometry and alluvial cover fraction. Then the experiment terminated.

The duration of the water surface elevation measurements was chosen by comparing water surface elevation estimates for different time intervals. The results of this analysis are presented in terms of mean and standard deviation of the water surface

elevation measurements in Table 2.2 for the cross section located 5 m downstream of the test reach entrance during a fully alluvial run with flow rate of 20 l/s and sediment feed rate of 400 g/min (Run 5).

Table 2.2 shows that the mean and standard deviation of the water surface elevation varied as the measurement duration increased from 5 to 25 minutes. The columns called *error* represent the percent error between the mean and the standard deviation for 5, 10, 15 and 20-minute long measurements, and the values of the 25-minute long measurement which were assumed to be our best estimate of the water surface elevation. After 20 minutes of measurement time the errors did not exceed 1%, i.e., 20 minutes was a sufficiently long measurement time to reasonably determine the water surface elevation. The same procedure was repeated for the bed elevation measurements and a duration of 30 minutes was chosen.

At the end of each experiment, I took pictures of the bed surface and sampled it to characterize the spatial changes in grain size distribution of the surface sediment. Each sample was 25 cm long and 19 cm wide and was collected by siphoning the deposit surface. The definition of bed surface in presence of bedforms is not straightforward. It can be defined as the 1-3 grain diameters thick layer of the bedforms stoss face (Blom et al., 2006) or it can be described as the bed layer with moving bedforms (Viparelli et al., 2013). In this study I used the latter definition because it was practically impossible to define a 1-3 diameter thick layer in the runs with exposed bedrock where portions of the channel bed were not entirely covered with alluvium. In other words, in the mixed bedrock-alluvial reaches, I assumed that the entire deposit represented the bed surface. Each sediment

sample was dried in the oven and then the grain size distribution was measured with sieve analysis.

2.3.2 Calculation of the flow characteristics at equilibrium

Equilibrium flow depths and velocities were determined from the measurements of water surface and bed elevation. Because water surface and bed elevation were measured in different locations, water surface elevation measurements were linearly interpolated to compute the flow depth H as the difference between the (interpolated) average water surface elevation and the measured bed elevations. The flow velocity U was then estimated as the ratio between the flow discharge and the cross-sectional area.

2.4 Results

The experimental results are presented in two sections: *alluvial equilibrium*, and *equilibrium with exposed bedrock*. Equilibrium conditions are described in terms of streamwise changes in standard deviation of the time series of bed elevation, water depth, and geometric mean grain size of the bed surface sediment. Measurements of water surface elevation and slope allowed us to characterize the spatial changes in flow velocity and resistances at equilibrium.

At equilibrium, the standard deviation of the time series of bed elevation σ_η is a measure of the variability of the bed elevation around its mean value, which is constant in time. In the case of equilibrium lower regime plane bed (i.e., no bedforms) σ_η increases with increasing bed shear stress (Wong et al., 2007). Here I used σ_η to quantify the

variability of bed elevation associated with bedload transport and downstream migrating bedforms.

The time series of bed elevation presented in Figure 2.3a was recorded at equilibrium during Run 3, i.e., the alluvial run with flow rate equal to 20 l/s, feed rate equal to 700 g/min and non-uniform bed material. The dashed grey line in Figure 2.3a represents the average bed elevation above the model bedrock. Two types of bed elevation changes can be identified, small amplitude, high frequency changes associated with bedload transport (Wong et al., 2007) and high amplitude, low frequency changes associated with downstream migrating bedforms. Figure 2.3a clearly shows that the magnitude of the bed elevation changes associated with bedform migration is orders of magnitude larger than the magnitude of the bed elevation changes associated with bedload transport, thus I used σ_η to characterize the bedform height: σ_η is largest in the experimental runs with largest bedforms.

In previous studies of mixed bedrock-alluvial river morphodynamics the alluvial cover fraction was defined as the aerial fraction of the bed covered with alluvium (Hodge et al., 2011; Inoue et al., 2014; Johnson, 2014). Due to the lack of sufficiently long time series of bed surface pictures, I defined the alluvial cover fraction based on the time series of bed elevation. A time series of equilibrium bed elevation in a mixed bedrock-alluvial reach is presented in Figure 2.3b, where the dashed grey line represents the mean bed elevation. The time series of Figure 2.3b was measured during Run 4, i.e., the run with flow rate equal to 20 l/s. feed rate equal to 700 g/min, non-uniform bed material and exposed bedrock at equilibrium. The high values of bed elevation correspond to periods

in which the bed was covered with alluvium, and the nearly constant low values of bed elevation identify periods of time in which the model bedrock was exposed.

Based on this information, I defined the alluvial cover fraction as the average fraction of time in which the model bedrock was covered with alluvium. Given the very limited changes in bedform shape within the 19 cm wide cross section, I assumed that the point measurement of alluvial cover fraction was representative of the entire cross section.

2.4.1 Alluvial equilibrium

The results of the alluvial equilibrium runs are presented in Figure 2.4 in terms of streamwise changes in 1) standard deviation of bed elevation σ_η (a, c, f, i), 2) average water depth H (b, d, g, j), and 3) geometric mean diameter of the bed surface sediment, D_{sg}, (e, h, k). The results of the run with uniform sand, flow rate equal to 20 l/s and feed rate equal to 700 g/min (Run 1) are presented in panels a and b. The results of the runs with non-uniform sand are in panels c-k. The results of Run 3, which had the same flow rate and feed rate of Run 1, are in panels c-e. Panels e-g summarize the results of the alluvial equilibrium run with flow rate equal to 20 l/s and feed rate equal to 400 g/min (Run 5); and panels i-k report the results of the alluvial equilibrium with flow rate equal to 10 l/s and feed rate equal to 400 g/min (Run 7). In Figure 2.4 the symbols denote measurements, the continuous lines are regression lines through the experimental points and the dashed grey lines in panels e, h and k represent the geometric mean diameter of the sediment feed.

The values of σ_η in Figure 2.4 revealed that the equilibrium bedform amplitude was not constant in the streamwise direction, as indicated with the red ovals in Figure 2.4 (a, c, f, i). In the upstream part of the test reach the bed was covered with relatively small

bedforms that grew as they moved in the streamwise direction until their heights and wavelengths became uniform for the rest of the flume length. The streamwise changes in equilibrium bedform height is shown in Figure 2.5 for Run 3, in terms of time series of bed elevation measurements (black lines). The dashed grey lines of Figure 2.5 represent the mean bed elevation. A time series collected in the upstream part of the test reach (1.81 m from the test reach entrance) is presented in Figure 2.5a, and a series collected in the downstream part of the flume (5.21 m from the test reach entrance) is in Figure 2.5b. The comparison between panels a and b clearly shows that the bedform height in the upstream part of the flume was smaller than in the downstream reach.

The region of the test reach in which the bedform amplitude grew in the streamwise direction is here called *bedform development region* and it is indicated with ovals in Figure 2.4. It is interesting to note that in the runs with non-uniform sediment (Figure 2.4c, f, and i) the bedform development region was ~2 m long while in Run 1 (Figure 2.4a), which was performed with uniform sand and the same flow and feed rates of Run 3, the bedform development region was ~4.5 m long.

The equilibrium flow depth is presented in Figure 2.4 (b, d, g and j). In all the experiments, the water depth increased in the streamwise direction in the bedform development region, and it became constant in space where the bedforms were fully developed. In the bedform development region σ_η, and thus the flow resistances, increased in the flow direction and this corresponded to increasing flow depths. The slopes of the regression lines of Figure 2.4 (b, d, g, j) are smaller than 0.001 m/m showing that water depth can be reasonably considered uniform downstream of the bedform development region.

The equilibrium D_{sg} is presented in Figure 2.4 (e, h, k) where the dashed grey lines represent the geometric mean size of the sediment feed and the slopes of the regression lines are smaller than 0.01 mm/m. The equilibrium bed surface was generally coarser than the sediment supply to regulate the mobility of the fine and coarse sediment (Parker and Klingeman, 1982; Paola et al. 1992). In the fully alluvial reach downstream of the bedform development region the equilibrium D_{sg} did not change in space.

2.4.2 Equilibrium with exposed bedrock

The results of the experiments with an equilibrium mixed bedrock-alluvial reach are summarized in Figure 2.6, which is analogous to Figure 2.4. Equilibrium data are presented in terms of streamwise changes in standard deviation of bed elevation σ_η (a, c, f, i), water depth H (b, d, g, j) and geometric mean diameter of the bed surface sediment D_{sg} (e, h, k). The results of the run with uniform sediment, flow rate equal to 20 l/s and feed rate equal to 700 g/min (Run 2) are in panels a-b. The results of the runs with non-uniform sand are in panels c-k. The results presented in panels c-e pertain to the run with flow rate equal to 20 l/s and feed rate equal to 700 g/min (Run 4). Panels f-h summarize the results of the run with flow rate equal to 20 l/s and feed rate equal to 400 g/min (Run 6). The results of the run with flow rate equal to 10 l/s and feed rate equal to 400 g/min (Run 8) are in panels i-k. In Figure 2.6 the symbols represent the experimental points, the grey lines are regression lines through the experimental points, the vertical lines denote the position of the stable alluvial-bedrock transition, and the black continuous lines denote equilibrium values for the paired (same flow rate, feed rate and sediment type, see Table 2.1) alluvial experiment downstream of the bedform development region.

Due to the limited length of the test reach, the downstream water surface base level in the mixed bedrock-alluvial runs was chosen so that the length of the alluvial reaches was of comparable length with the bedform development region observed in the fully alluvial runs with non-uniform bed material, i.e., ~ 2 m (Figure 2.4).

Figure 2.6 (a, c, f, i) shows the streamwise variation of σ_η at equilibrium. In Run 2 (Figure 2.6a) σ_η grew in the alluvial reach with values that were comparable with those measured in the paired fully alluvial equilibrium run (Run 1). Due to the interaction with the model bedrock σ_η decreased in the flow direction in the mixed bedrock-alluvial reach (0.051 m/m). A similar streamwise decrease of σ_η (0.07 m/m) was observed in Run 8 (flow rate 10 l/s and feed rate 400 g/min, Figure 2.6i). In Run 4, which was performed with the same flow rate and feed rate of Run 2 but with non-uniform sand, σ_η was smaller than in the paired fully alluvial run and gently (0.022 m/m) decreased in the streamwise direction in the mixed bedrock-alluvial reach. Finally, in Run 6 with flow rate equal to 20 l/s and feed rate equal to 400 g/min σ_η did not seem to significantly change from the alluvial equilibrium value and remained uniform in the mixed bedrock-alluvial reach (0.009 m/m) (Figure 2.6f).

Panels b, d, g, j show the changes in water depth in the mixed bedrock-alluvial reaches compared to the fully alluvial cases. In the runs with feed rate equal to 700 g/min, i.e. Run 2 and Run 4 (Figure 2.6 b, d), a change in water depth compared to the paired fully alluvial runs is clearly visible. In particular, in the run with uniform bed material (Run 2) the water depth at the end of the alluvial reach was similar to the water depth in the corresponding fully alluvial run (Run1) and the interaction with the model bedrock resulted

in a water depth that decreased in the flow direction of 0.0028 m/m (Figure 2.6b). In the run with non-uniform bed material and a feed rate equal to 700 g/min (Run 4), the water depth at the end of the alluvial reach was smaller than in the paired alluvial run (Run 3) and then it gently decreased (0.0019 m/m) in the streamwise direction in the mixed bedrock-alluvial reach (Figure 2.6d). In the runs with a feed rate equal to 400 g/min, i.e., Run 6 and 8, (Figure 2.6 g and j) the water depths decreased very gently in the flow direction in the mixed bedrock-alluvial reach (0.0018 m/m in run 6 and 0.0023 m/m in Run 8).

The response of the flow to the presence of the model bedrock in the experimental runs showed that the distance between the water surface base level and the bedrock plays a prime control on the flow characteristics in the mixed bedrock-alluvial reach. In Runs 2 and 4 the distance between the water surface base level and the model bedrock was respectively equal to 80% and 90% of the alluvial equilibrium depth in the paired runs H_o, and this forced the equilibrium flow depth to clearly decrease in the streamwise direction compared to the fully alluvial case. In Runs 6 and 8 the distance between the water surface base level and the model bedrock was respectively equal to $0.97H_o$ and H_o, not enough to cause a visible flow acceleration in our relatively short test reach.

Panels e, h, k show the spatial changes of D_{sg} in the streamwise direction. In Runs 4 and 8 there was no significant change of D_{sg} compared to the alluvial equilibrium runs, but a very mild pattern of downstream fining was observed in Run 4 (0.01 mm/m in Run 4 and 0.0034 mm/m in Run 8). On the contrary, in Run 6 (flow rate 20 l/s and feed rate 400 g/min) a clear pattern of downstream fining was observed in the mixed bedrock-alluvial reach (0.051 mm/m) (Figure 2.6h). These results suggest that in the runs in which the σ_η

decreased in streamwise direction, i.e., Runs 4 and 8, there was a small streamwise change of the geometric mean diameter of the surface material compared to the paired alluvial runs. On the other hand, in the run with σ_η close to the alluvial equilibrium value, a stable pattern of downstream fining formed on the bed surface.

The spatial change in alluvial cover at equilibrium is presented in Figure 2.7, where the black crosses refer to Run 2, the grey triangles to Run 4, the black diamonds to Run 6 and the grey circles to Run 8. When the alluvial cover was equal to 1, the reach was fully alluvial, and exposed bedrock was observed when the alluvial cover is smaller than 1. Significant changes in alluvial cover fraction between the experimental runs were not observed suggesting that the streamwise distance between the alluvial-bedrock transition and the end of the test reach might have had a significant control on the fraction of exposed bedrock.

2.4.3 Summary of the experimental results

In our experiments the interaction of the bedrock surface with the flow hydrodynamics and the sediment transport processes varied depending on the vertical distance between the water surface base level and the bedrock surface. When this distance was close to the alluvial equilibrium flow depth H_o (Runs 6 and 8) significant streamwise changes in flow depth and flow velocity from the alluvial equilibrium values were not observed in the mixed bedrock-alluvial reach. On the contrary, when the vertical distance between the water surface base level and the underlying model bedrock was significantly smaller than the alluvial equilibrium depth, a shallower flow depth than in the paired

alluvial runs and spatial flow acceleration was observed in the mixed bedrock-alluvial reaches (Figures 2.6b and d).

The observed spatial changes in water depth partially confirm the numerical predictions of the Viparelli et al. (2015) formulation, i.e., at equilibrium in a low slope mixed bedrock-alluvial reach downstream of an alluvial-bedrock transition the flow is characterized by a reduction of the flow depth in the streamwise direction. The results also showed that the problem is more complex than in the Viparelli et al. (2015) formulation due to changes in bedform geometry and grain size distribution of the alluvial bed surface, which may occur with very small changes in flow depth and velocity.

In a sediment feed flume the equilibrium bedload transport rate must be equal to the sediment feed rate (equation 2-1). Due to the presence of exposed bedrock, the bed material transport capacity in the mixed bedrock-alluvial reaches should be higher than the bed material transport capacity in the alluvial reaches (Sklar and Dietrich, 2004; Zhang et al., 2015). Recalling that the bed material transport capacity is an increasing function of the bed shear stress associated with skin friction (Fernandez Luque and Van Beek, 1976; Parker, 2008), I hypothesized that the observed changes in bedform geometry and grain size distribution of the bed surface sediment result in higher bedload transport capacities than in the corresponding fully alluvial runs.

The interaction between the flow hydrodynamics, the bedload transport and the model bedrock resulted in two different responses, a streamwise decrease in σ_η in Runs 2, 4 and 8 and the formation of a stable pattern of downstream fining in Runs 4 and 6. It is important to note here that in Run 4, both the streamwise decrease in σ_η and the pattern of

downstream fining were milder than those observed in the other runs, which were either characterized by a change in σ_η or by downstream fining of the bed surface sediment.

Noting that 1) the vertical distance between the water surface base level and the model bedrock in Runs 6 and 8 was very close to the alluvial equilibrium values, 2) Run 6 was characterized by uniform σ_η and a stable pattern of downstream fining, and 3) σ_η decreased in the streamwise direction without spatial changes of D_{sg} in Run 8, I hypothesized that the vertical distance between the water surface base level and the bedrock surface cannot be the only control on bedform regime and the sediment sorting patterns in the mixed bedrock-alluvial reach.

2.5 Discussion

To test the hypotheses presented above, the discussion section is organized in three parts. In part 1, I computed the spatial changes in flow resistances and bed shear stresses in the mixed bedrock-alluvial reach to determine if the observed changes in bedform geometry and grain size distribution of the bed surface sediment correspond to higher bedload transport capacities than at alluvial equilibrium. The bed shear stresses computed in part 1 are then used to determine if size-specific bedload transport relations for fully alluvial systems can be reasonably applied to model bedload transport of non-uniform sediment in mixed bedrock-alluvial reaches. Finally, in part 3, I used one of the Vanoni (1975) bedform diagrams to compare the bedform characteristics observed in the bedrock reaches with those observed in the paired fully alluvial cases.

2.5.1 Spatial changes in flow resistances and in bed shear stress in the mixed bedrock-alluvial reaches

In the experiments presented in Sections 3 and 4, either the grain size distribution of the bed surface sediment, the bedform geometry in the mixed bedrock-alluvial reaches, or both were different from those measured at equilibrium in the paired alluvial runs. I thus expected that the flow resistances and consequently the bed shear stresses in the mixed bedrock-alluvial runs are different from their alluvial equilibrium values.

The calculation of the bed shear stress and of the flow resistances was not straightforward. To account for the different roughness between the smooth sidewalls and the rough bed the procedure suggested by Vanoni and Brooks (1957) was followed, as summarized in A.1 of the Appendix A. Further, to distinguish between the bed resistances associated with the presence of an alluvial bed with exposed bedrock the flow resistances have been partitioned as illustrated below following Johnson (2014). Finally, the alluvial resistances have been partitioned between skin friction and form drag with an Einstein decomposition of the sidewall corrected alluvial values, as illustrated in Appendix A (Parker, 2004).

The results of this analysis are presented in Figure 2.8 in terms of total, sidewall corrected friction coefficients in the bed region $C_{f,b}$ (panels a, d, g, j), friction coefficients associated with skin friction on the alluvial patches, $C_{f,bas}$ (panels b, e, h, k) and sediment transport capacity in mixed bedrock-alluvial reaches Q_{bT} (panels c, f, i, l). The experimental results of Figure 2.8 (a-c) pertain to Run 2, those in Figure 8 (d-g) to Run 4, the data in Figure 2.8 (h-j) are of Run 6 and the data in Figure 2.8 (i-l) are from Run 8. The

red ovals identify the mixed bedrock-alluvial reaches; the horizontal lines represent the equilibrium values of the corresponding fully alluvial runs.

a) Spatial changes in total (sidewall corrected) bed friction coefficient

Panels a, d, g, j of Figure 2.8 show that the total, sidewall corrected friction coefficient, $C_{f,b}$ in the runs with exposed bedrock decreases in the streamwise direction. There are two reasons associated with this 1) the decrease in roughness height caused by the downstream fining of the bed surface material (Runs 4 and 6) and by the streamwise decrease in σ_η (Runs 2, 4 and 8), and 2) an increase of the aerial fraction of the exposed bedrock, which was characterized by a smaller roughness height than the alluvial patches. The characteristic roughness height of the model bedrock was ~0.1 mm and the grain roughness height of the alluvial patches was assumed to be a function of D_{s90}, i.e., the diameter such that 90% of the bed surface sediment was finer. Therefore, as the fraction of exposed bedrock increased, the composite roughness became smaller so that the friction coefficient decreased in streamwise direction for all mixed bedrock-alluvial runs.

b) Spatial changes in flow resistances associated with skin friction

In the Johnson (2014) formulation to compute flow resistances in mixed bedrock-alluvial reaches, the friction coefficient for the bed region was defined as a weighted average between the friction coefficient for the alluvium and for the exposed bedrock

$$C_{f,b} = p_c C_{f,ba} + (1 - p_c) C_{f,bb} \tag{2-2}$$

where $C_{f,ba}$ was the friction coefficient associated with the alluvium and $C_{f,bb}$ is the friction coefficient associated with the bedrock. To partition the flow resistances between the alluvial patches and the exposed bedrock I applied a procedure similar to the procedure

used to partition the flow resistances in alluvial rivers between skin friction and form drag (Parker, 2004 and references therein). I considered an ideal flow over a rough bed with the same roughness of the bedrock surface. The energy slope and mean flow velocity of this ideal flow were assumed to be equal to the energy slope and the mean flow velocity of the flow in presence of alluvial patches, i.e., of the experimental runs. The friction coefficient for the exposed bedrock was thus computed as

$$C_{f,bb}^{-1/2} = \alpha_r \left(\frac{r_{b,b}}{k_{sb}}\right)^{1/6} \tag{2-3}$$

with k_{sb} denoting the roughness height of the bedrock (0.1 mm), and $r_{b,b}$ the hydraulic radius of the ideal flow over the bedrock surface. Using a Manning-Strickler formulation, $r_{b,b}$ was computed as

$$r_{b,b} = \left(\frac{k_{sb}^{1/6} U}{\alpha_r \sqrt{g s_f}}\right)^{3/2} \tag{2-4}$$

with U being the cross sectionally averaged flow velocity and S_f the friction slope. Using equations (2-2) - (2-4) I computed the friction coefficient of the alluvial zones, which accounts for flow resistances associated with both skin friction and form drag $C_{f,ba}$. I then partitioned the alluvial flow resistances between skin friction and form drag, as illustrated in the Supplementary Information, to estimate the friction coefficient associated with skin friction $C_{f,bas}$, which is necessary to perform bedload transport calculations. Panels b, c, h, k of Figure 2.8 shows the spatial variation of the friction coefficient associated with skin

friction for the alluvial areas, which in the mixed bedrock-alluvial reaches is gently decreasing in streamwise direction.

c) Spatial changes in sediment transport capacity in the mixed bedrock-alluvial reach

The sediment transport capacity Q_{bT} was computed with the relation of Ashida and Michiue as outlined in Parker (2008) for uniform material equal to the geometric mean size of the sediment feed D as

$$Q_{bT} = B\sqrt{RgD}D \cdot 17(\tau^*_{bas} - 0.05)\left(\sqrt{\tau^*_{bas}} - \sqrt{0.05}\right) \quad (2\text{-}5)$$

where B is the flume width, R denotes the submerged specific gravity of the sediment equal to 1.65 in the calculations presented herein, g is the acceleration of gravity and τ^*_{bas} represents the Shields number on the alluvial patches associated with skin friction, equal to the $C_{f,bas}U^2/RgD$.

The streamwise variability of Q_{bT} in the runs with exposed bedrock is presented in Figure 2.8 (c, f, i, l). In the mixed bedrock-alluvial reaches Q_{bT} clearly increases in the streamwise direction. This corresponds to the reduction of alluvial cover of Figure 2.7.

The results of Figures (2.6) - (2.8) show that the response of the flow and of the bedload transport to the presence of an un-erodible surface is more complex than that presented in Zhang et al. (2015) and Viparelli et al. (2015). Notwithstanding the streamwise reduction of the flow resistances (Figure 2.8 a, b, d, e, g, h, j, k), downstream of the stable alluvial-bedrock transitions the bed material transport capacity tends to increase in the direction of the flow (Figure 2.8 c, f, i, l).

2.5.2 Comparison between the experimental results and the Ashida and Michiue bedload transport relation

To determine if surface-based bedload relations for fully alluvial systems can be reasonably used to predict grain size specific bedload transport rates in mixed bedrock-alluvial reaches, I compared our experimental data with bedload transport rates predicted using the surface-based version of the Ashida and Michiue relation (Parker, 2008), which is appropriate to model bedload transport in alluvial reaches transporting sand and pea gravel.

The surface-based form of the Ashida and Michiue bed load relation takes the form

$$q^*_{bsi} = 17(\tau^*_{bsi} - \tau^*_{refi})(\sqrt{\tau^*_{bsi}} - \sqrt{\tau^*_{refi}}) \quad (2\text{-}6)$$

where q^*_{bsi} represents dimensionless transport rate per unit width of sediment with characteristic grain size D_i, τ^*_{bsi} is the size-specific Shields number associated with skin friction defined as the ratio between the alluvial bed shear stress associated skin friction and ρRgD_i, with ρ being the water density, R the submerged specific gravity of the sediment and g the acceleration of gravity, and τ^*_{refi} denotes reference Shields number for the sediment particles with characteristic grain size D_i, computed with the following hiding/exposure function (Parker, 2008)

$$\frac{\tau^*_{refi}}{\tau^*_{scg}} = \begin{cases} 0.843\left(\frac{D_i}{D_{sg}}\right)^{-1} for \frac{D_i}{D_{sg}} \leq 0.4 \\ \left[\frac{log(19)}{log\left(19\frac{D_i}{D_{sg}}\right)}\right]^2 for \frac{D_i}{D_{sg}} < 0.4 \end{cases} \quad (2\text{-}7)$$

in which τ^*_{scg} is a reference value equal to 0.05.

The grain size specific volumetric bedload transport rate per unit channel width is computed using the definition of dimensionless transport rate per unit channel width as

$$q_{bi} = \sqrt{RgD_i} D_i p_c F_i q^*_{bsi} \quad (2\text{-}8)$$

where F_i denotes the volume fraction content of sediment with characteristic grain size D_i in the bed surface. The only difference of this relation with relations for fully alluvial systems is the presence of p_c in the right-hand side, which accounts for the reduced availability of alluvial sediment associated with the presence of exposed bedrock. The total sediment transport rate per unit width is then computed as the sum of q_{bi} over all the grain size fractions

$$q_{bT} = \sum_{i=1}^{n} q_{bi} \quad (2\text{-}9)$$

where n denotes the number of characteristic grain sizes.

The comparison between experimental and computed bedload transport rates is presented in Figure 2.9, where the black squares represent the alluvial equilibrium

experiments and the grey triangles refer to equilibrium conditions in the mixed bedrock-alluvial reaches. The equilibrium bedload transport rate in the experiments, which was equal to the sediment feed rate, is on the horizontal axis of Figure 2.9, while the results of the calculations performed with equations (2-6) - (2-9) are reported on the vertical axis. The continuous line represents perfect equality and the dashed lines identify the 50% error from the measured value.

The difference between experimental and predicted values of bedload transport rates is in the majority of the cases within the ± 50% error, which is comparable with the error of other bedload transport rate predictors for non-uniform sediment (Parker, 1990; Wilcock and Crowe, 2003). Thus, the surface-based version of the Ashida and Michiue bedload transport relation reasonably reproduces the bedload transport rates measured during the experiments. It is expected that other bedload transport models derived for alluvial systems can be used to predict the total, i.e., summed over all the grain sizes, bedload transport rates in mixed bedrock-alluvial rivers if the bedload transport capacity is multiplied by the alluvial cover fraction (Sklar and Dietrich, 2004).

To determine if the Ashida and Michiue surface-based relation was able to adequately model the grain size specific sediment fluxes, I used equations (2-6) - (2-9) to predict the equilibrium grain size distribution of the surface material in the mixed bedrock-alluvial reaches, as outlined by Parker and Southard (1990) for fully alluvial systems. The only difference between the procedure used herein and that presented by Parker and Southard (1990) is that our grain size specific bedload transport capacities are multiplied by the alluvial cover fraction p_c.

The comparison between predicted and measured grain size distributions of the bed surface sediment is presented in Figure 2.10 for three different locations i.e., ~ 0.81 m, ~ 2.81 m, and ~ 4.81 m from the test reach entrance. The black diamonds in Figure 2.10 denote experimental measurements, the continuous lines are model predictions and the error bars indicate 10% error. The comparison between model predictions and experimental data reveals a reasonably good agreement between measured and predicted equilibrium grain size distributions of the bed surface sediment in the middle and downstream locations, i.e., where the bedforms are fully developed. The prediction errors of the grain size distributions of the bed surface sediment are comparable with those of surface-based models in alluvial systems (e.g. Parker and Southard, 1990). These results further confirm that grain size specific bedload transport models derived for fully alluvial systems can be reasonably used to model grain size specific bedload transport in mixed bedrock-alluvial reaches if the bed material transport capacities are multiplied by the alluvial cover.

2.5.3 Changes in bed configuration

To test the hypothesis that the observed changes in σ_η and/or grain size distribution of the bed surface sediment are not solely controlled by the vertical distance between the water surface base level and the bedrock surface, I used the Vanoni (1975) diagram for sediment sizes of 0.93 mm, 1.2 mm and 1.35 mm. The vertical axis of the Vanoni (1975) diagram is Froude number, defined as $U/(gH)^{0.5}$ with U denoting the mean flow velocity, g acceleration of gravity and H the flow depth. The horizontal axis is the ratio between water depth and grain size of the bed material, set equal to D_{sg} in the runs with non-uniform sediment.

The Vanoni (1975) diagram is presented in Figure 2.11 where the black lines represent the transition between dunes and antidunes (Vanoni, 1975) and the symbols are our experimental points. The experimental results of the fully alluvial runs, i.e Runs 1, 3, 5 and 7, are respectively shown with blue, red, green and purple squares. The results of Run 2 are indicated with blue stars and those of Run 4 with red plus signs, the green triangles refer to Run 6, and the purple diamonds pertain to Run 8.

In Runs 2, 4 and 8, which were characterized by smaller values of σ_η in the mixed bedrock-alluvial reaches than in the paired fully alluvial runs, the bedform diagram of Figure 2.11 suggests that the observed change in bedform shape was associated with a change in bed configuration from the dune regime toward upper regime plane bed at the dune-antidune transition. In Run 6 significant changes in σ_η from the alluvial equilibrium case were not observed and this corresponded to no significant change in the bedform regime at equilibrium in the mixed bedrock-alluvial reach (green triangles in Figure 2.11).

Recalling that the distance between water surface base level and the bedrock surface in Runs 2, 4, 6 and 8 was respectively equal to $0.8H_o$, $0.9H_o$, $0.97H_o$ and H_o, respectively, Figure 2.11 suggests that when the distance between the water surface base level and the bedrock surface is significantly smaller than the alluvial equilibrium flow depth (Runs 2, blue asterisks, and Run 4, red plusses), the interaction between the bedrock surface and the bedforms results in bedform configurations that are closer to the dune-antidune transition and with smaller bedform heights than in the fully alluvial case. When the distance between the water surface base level and the bedrock surface is close to the equilibrium flow depth and the bedform regime is close to the dune-antidune transition (Run 8, purple diamonds), the interaction between the bedrock surface and the bedforms

results in bedform characteristics that are closer to antidunes than in the alluvial case. When the distance between the water surface base level and the bedrock surface is close to the alluvial equilibrium flow depth and the bedforms are well in the dune regime (Run 6, green triangles), no changes in σ_η and bedform regime should be expected. Finally, when the alluvial equilibrium bed configuration is far from the dune-antidune transition (Runs 3 and 5), the formation of a stable pattern of downstream fining in the mixed bedrock-alluvial reach can be expected (Runs 4 and 6).

New experiments and field data are necessary to confirm these observations and fully understand the complex interaction between bedload transport of non-uniform material and bedform characteristics in low slope, sand bed mixed bedrock-alluvial reaches.

2.6 Conclusions

I performed laboratory experiments on the equilibrium of low slope mixed bedrock-alluvial channels transporting non-uniform sand. The experiments provided novel and quantitative insight on the flow characteristics, bedform geometry, longitudinal sorting patterns and flow resistances in mixed bedrock-alluvial reaches, notwithstanding the limited length of the test reach.

In equilibrium mixed bedrock-alluvial reaches downstream of an alluvial-bedrock transition, i.e., when the slope of the bedrock surface is milder than the equilibrium slope of an alluvial system subject to the same flow regime and sediment supply, the interaction between the hardily erodible bedrock, the flow characteristics and the sediment transport may result in:

- flow acceleration (Figure 2.6 b, d, g and j) in the streamwise direction due to the limited space to store sediment on the channel bed and to convey the flow. This spatial flow acceleration is associated with a decreasing alluvial cover in the direction of the flow;

- changes in bedform geometry compared to the alluvial equilibrium case. In mixed bedrock-alluvial reaches σ_η tends to be smaller than in the fully alluvial case and, due to the flow acceleration, it may decrease in the flow direction (Figure 2.6 a, c, f, i);

- formation of a stable pattern of downstream fining of the bed surface sediment in response to the flow acceleration in the mixed bedrock-alluvial reach (Figure 2.6 e, h, k). This can be explained noting that as bedload transport capacity increases in the streamwise direction, the bed surface tends to become un-armored (Parker and Klinegman, 1982);

The observed streamwise decrease in σ_η and/or bed surface grain size observed in the experiments results in a streamwise decrease in the flow resistances. This streamwise decrease of the flow resistances is associated with an increase of the bed material transport capacity in the mixed bedrock-alluvial reach, which balances the streamwise reduction in alluvial cover fraction.

Surface-based formulations of grain size specific bedload transport models are able to reasonably reproduce the grain size specific bedload transport rates in mixed bedrock-alluvial reaches, if the alluvial cover is used to balance the higher bedload transport capacities associated with the spatial flow acceleration.

The response of the bedforms and of the bed surface sediment to the presence of a non-erodible surface seems to depend on the vertical distance between the water surface base level and the bedrock surface and to the bedform regime (Figure 2.11). If the vertical distance between the water surface base level and the bedrock surface is significantly smaller than the alluvial equilibrium flow depth or the alluvial equilibrium bedforms in are close to the dune-antidune transition, a streamwise reduction in σ_η can be expected in the mixed bedrock-alluvial reach. If the alluvial equilibrium bedforms are well in the dune regime and the vertical distance between the downstream water surface base level and the bedrock surface is close to the alluvial equilibrium flow depth, the formation of a stable pattern of downstream fining of the bed surface sediment in the mixed bedrock-alluvial reach can be expected.

Table 2.1 Experimental conditions

Run	Flow Rate (l/s)	Feed Rate (g/min)	ζ_d (m)	Grain Size	Condition
1	20	700	0.173	Uniform	Fully alluvial
2	20	700	0.166	Uniform	Mixed bedrock-alluvial
3	20	700	0.164	Non-uniform	Fully alluvial
4	20	700	0.148	Non-uniform	Mixed bedrock-alluvial
5	20	400	0.186	Non-uniform	Fully alluvial
6	20	400	0.177	Non-uniform	Mixed bedrock-alluvial
7	10	400	0.088	Non-uniform	Fully alluvial
8	10	400	0.081	Non-uniform	Mixed bedrock-alluvial

Table 2.2 Average water surface elevation and standard deviation of the water surface elevation for different measurement durations in Run 5 at 5 m from the test reach entrance

Time (min)	**Average water depth**		**Standard deviation**	
	Value (cm)	Error %	Value (cm)	Error %
5	21.8	0.1	0.28	34.6
10	22.0	0.7	0.35	19.9
15	22.0	0.9	0.36	17.5
20	21.8	0.2	0.44	0.8
25	21.8		0.43	

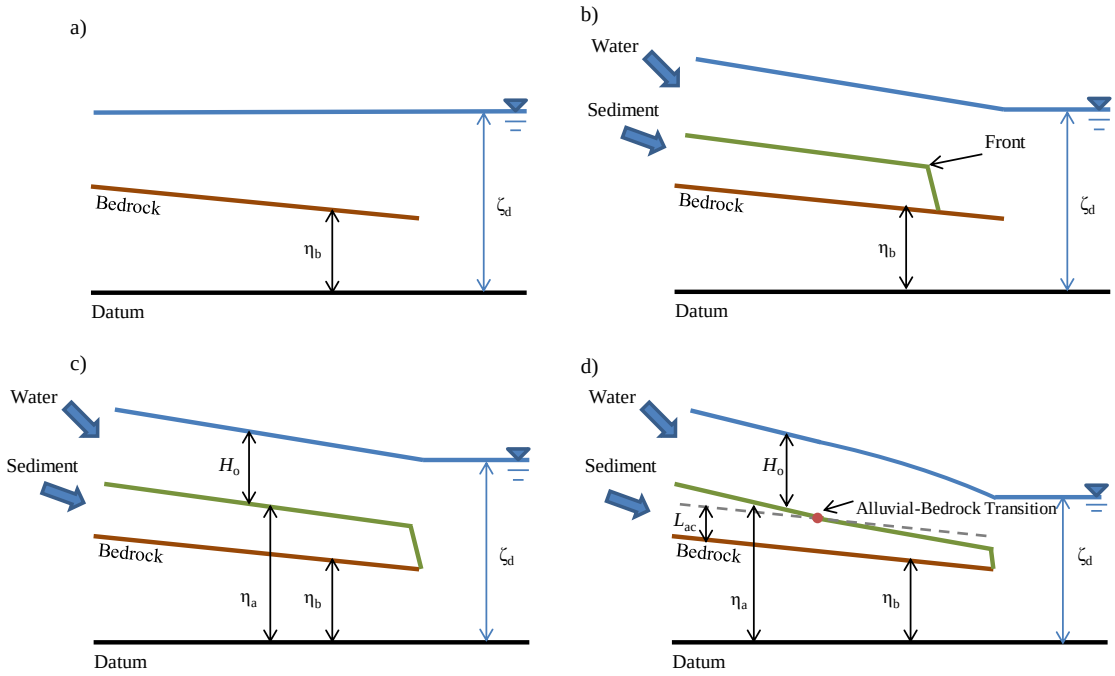

Figure 2.1 schematic illustration of the evolution of an alluvial deposit in a sediment feed flume. a) empty flume with standing water, b) alluvial deposit with a downstream migrating front, c) alluvial equilibrium, d) equilibrium with an alluvial-bedrock transition. η_b represents the bedrock elevation, η_{bd} denotes the bedrock elevation at the downstream end of the channel, η is the alluvial bed surface elevation, H_o is the alluvial equilibrium water depth, ζ_d is the water level at the downstream end and L_{ac} represents the minimum thickness of alluvial cover

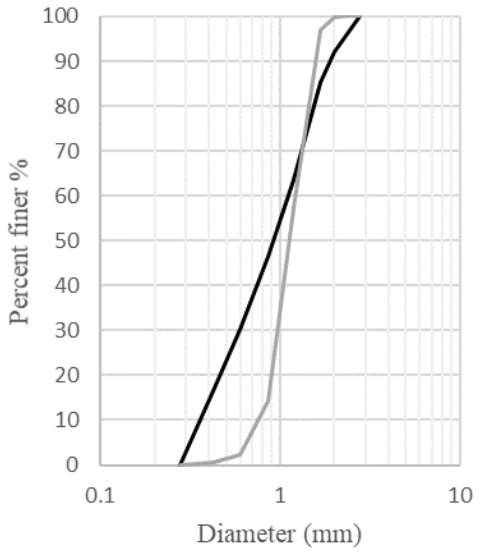

Figure 2.2 Grain size distribution of the material used in the experiments. The grey line is the uniform material used in Runs 1 and Runs 2. The black line represents the non-uniform material used in Runs 3-8.

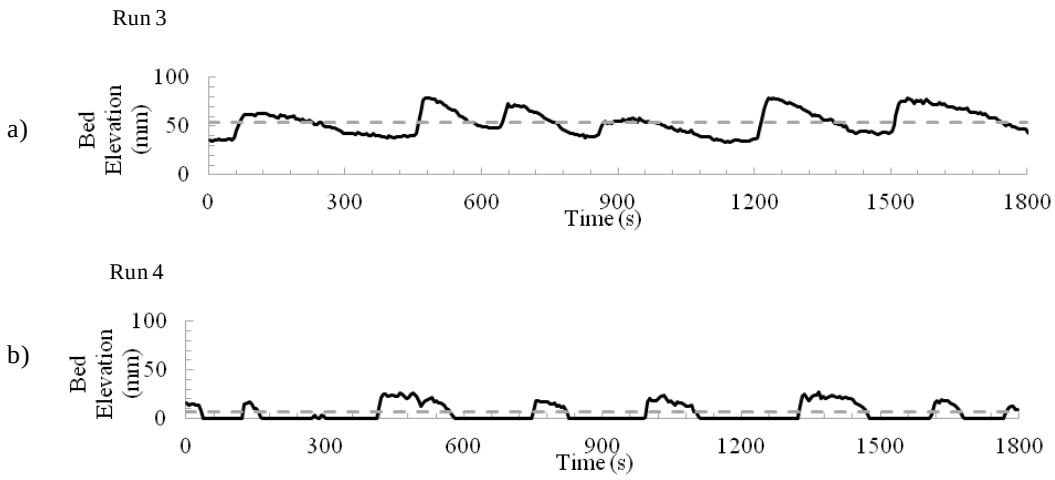

Figure 2.3 Time series of bed elevation fluctuations (a) Run 3 (700 g/min, 20 l/s, non-uniform material, alluvial run) at 5.21 m from the test reach entrance. (b) Run 4 (700 g/min, 20 l/s, non-uniform material, equilibrium with exposed bedrock) at 5.21 m from the test reach entrance. The dashed gray line indicates average bed elevation.

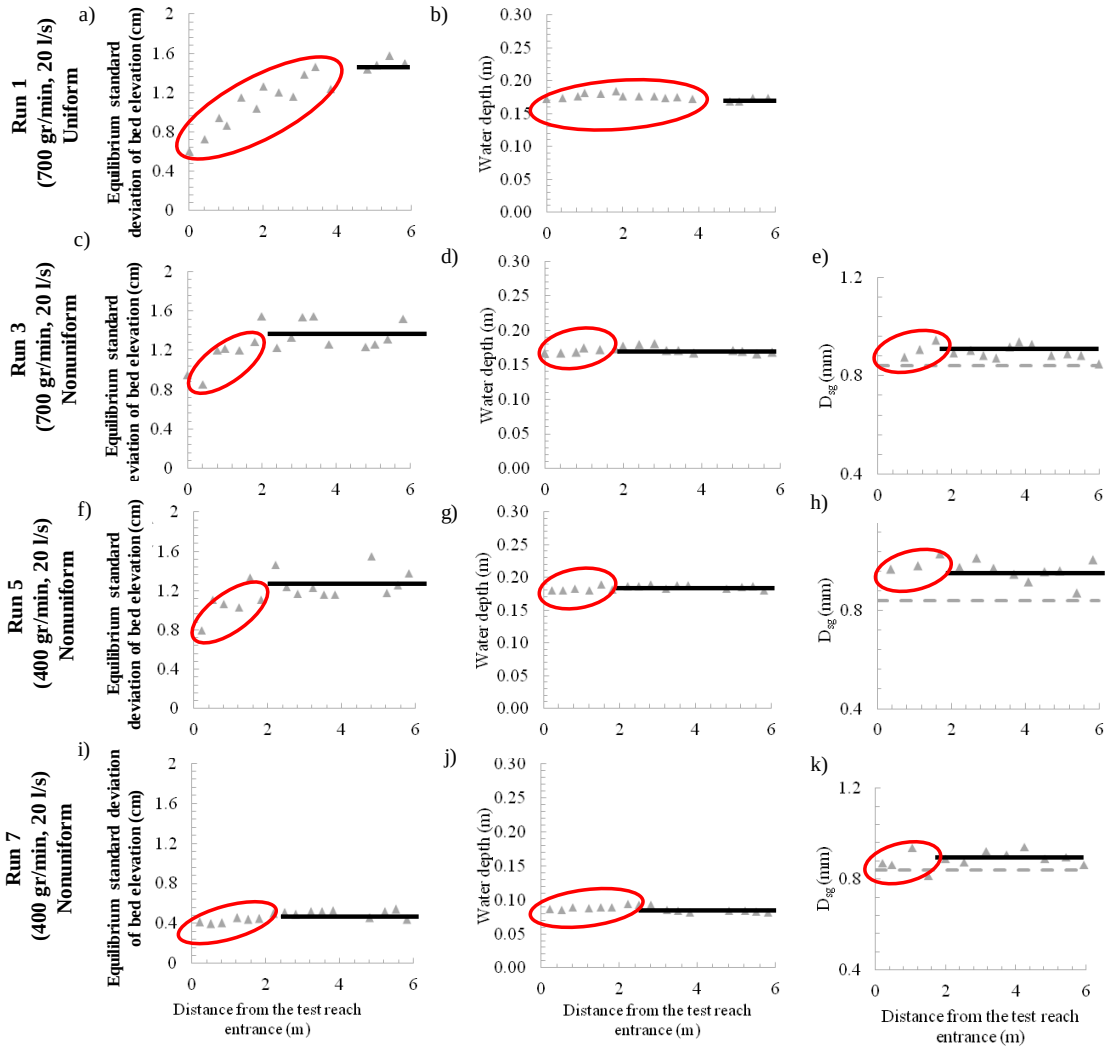

Figure 2.4 Spatial changes in equilibrium standard deviation of the bed elevation, σ_η, water depth, H, and geometric mean diameter of the surface sediment, D_{sg}, in the fully alluvial runs (Runs 1, 3, 5 and 7). Symbols represent the experimental points. The black lines are the regression lines through the experimental points. The dashed grey line in the D_{sg} plots represents the geometric mean size of the sediment feed. Red ovals qualitatively indicate the bedform development region.

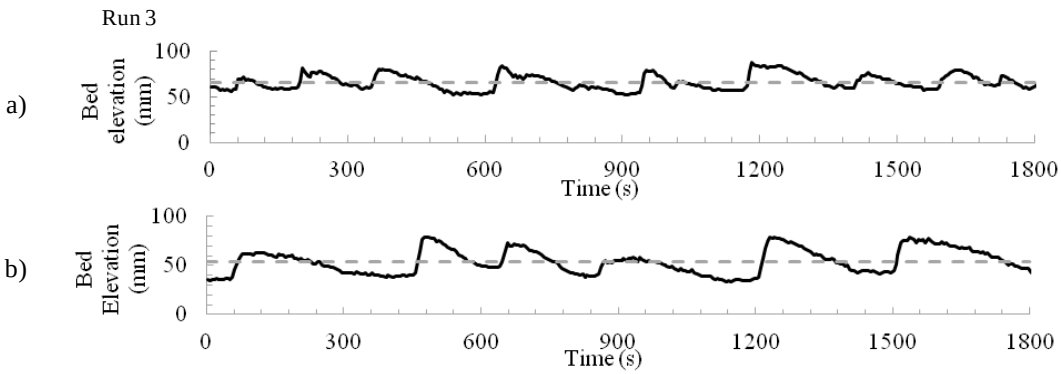

Figure 2.5 Time series of the bed elevation fluctuations in Run 3 (700 g/min, 20 l/s, non-uniform material, alluvial equilibrium). a) Measurements at 1.81 m from the test reach entrance. b) Measurements at 5.21 m from the test reach entrance. The solid lines are the sonar measurements and the dashed grey line is the time averaged bed elevation.

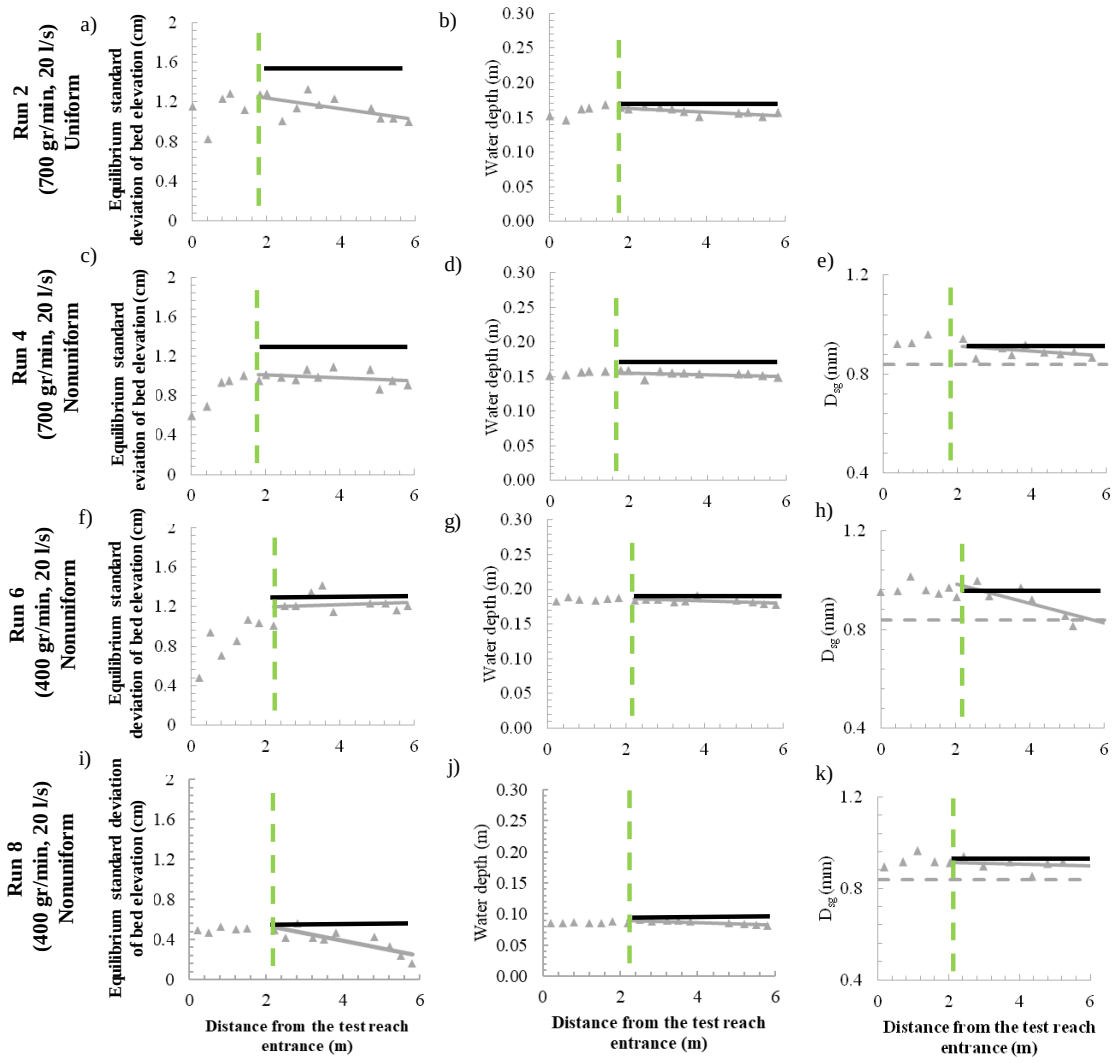

Figure 2.6 Spatial changes in equilibrium standard deviation of the bed elevation, σ_η, water depth, H, and geometric mean diameter of the surface sediment, D_{sg}, in the runs with exposed bedrock (Runs 2, 4, 6 and 8). Symbols represent the experimental points. The black lines are the fully alluvial values downstream of the bedform development region. The dashed green lines indicate the location of the stable alluvial-bedrock transition. The grey lines are regression lines on the exposed bedrock data points.

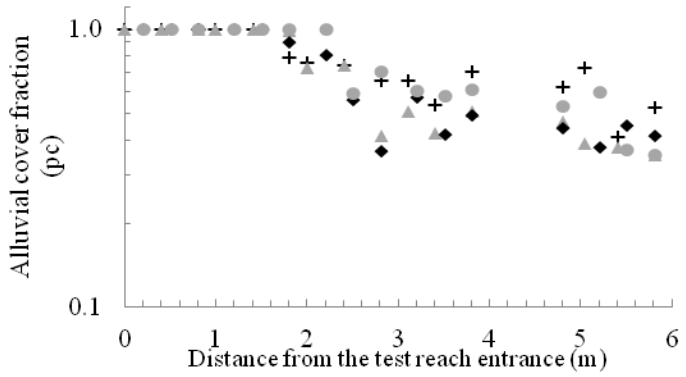

Figure 2.7 Streamwise changes of the equilibrium alluvial cover fraction, p_c. Black pluses, grey triangles, black diamonds and grey circles respectively represent p_c for Run 2 (700 g/min, 20 l/s, uniform), Run 4 (700 g/min, 20 l/s, non-uniform), Run 6 (400 g/min, 20 l/s, non-uniform) and Run 8 (400 g/min, 10 l/s, non-uniform).

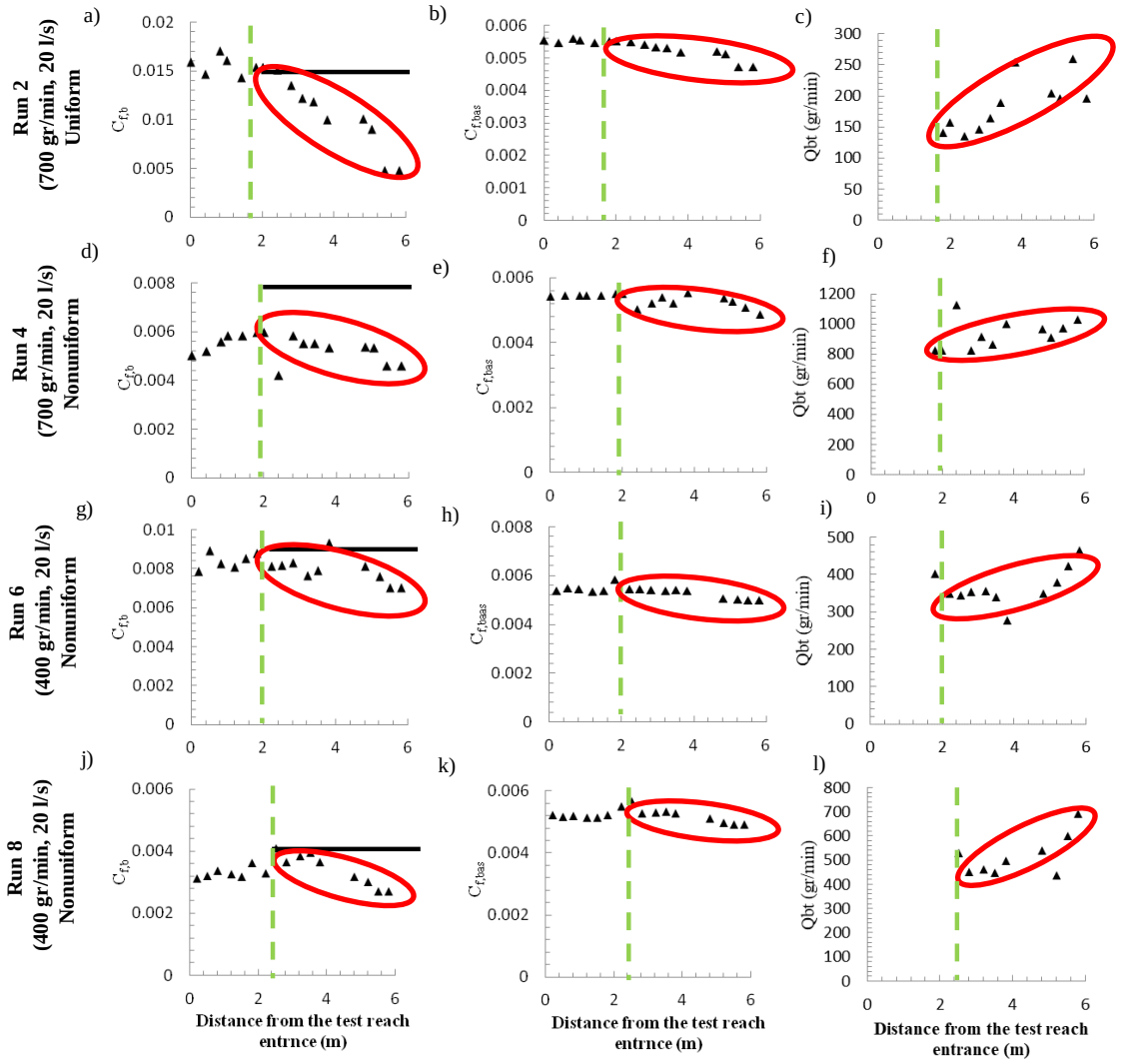

Figure 2.8 streamwise changes of the equilibrium total, sidewall corrected friction coefficient $C_{f,b}$ (a, d, g, j), friction coefficient associated with skin friction for the alluvial patches, $C_{f,bas}$ (b, e, h, k), and Sediment transport capacity over the exposed bedrock reach, Q_{bT} (c, f, i, l). The green line denotes the location of alluvial-bedrock transition. The black lines represent fully alluvial values downstream of the alluvial-bedrock transition and the red ovals show the values in exposed bedrock runs downstream of the alluvial-bedrock transition.

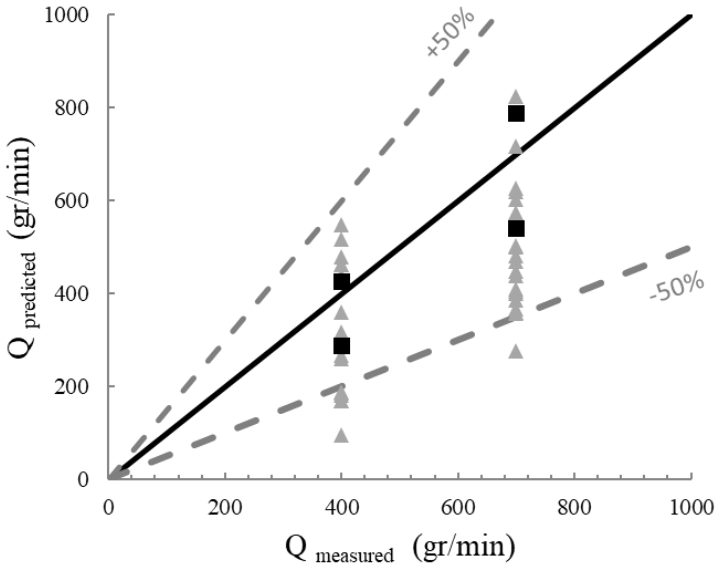

Figure 2.9 Comparison between the measured (horizontal axis) and predicted (vertical axis) bedload transport rates per unit width. Predictions are done with the Ashida and Michiue bedload relation multiplied by the measured alluvial cover fraction. The grey triangles are the points pertaining to experimental runs with exposed bedrock and the black squares represent fully alluvial runs. The black line corresponds to perfect equality and the dashed lines indicate $\pm$50% difference between measured and predicted values.

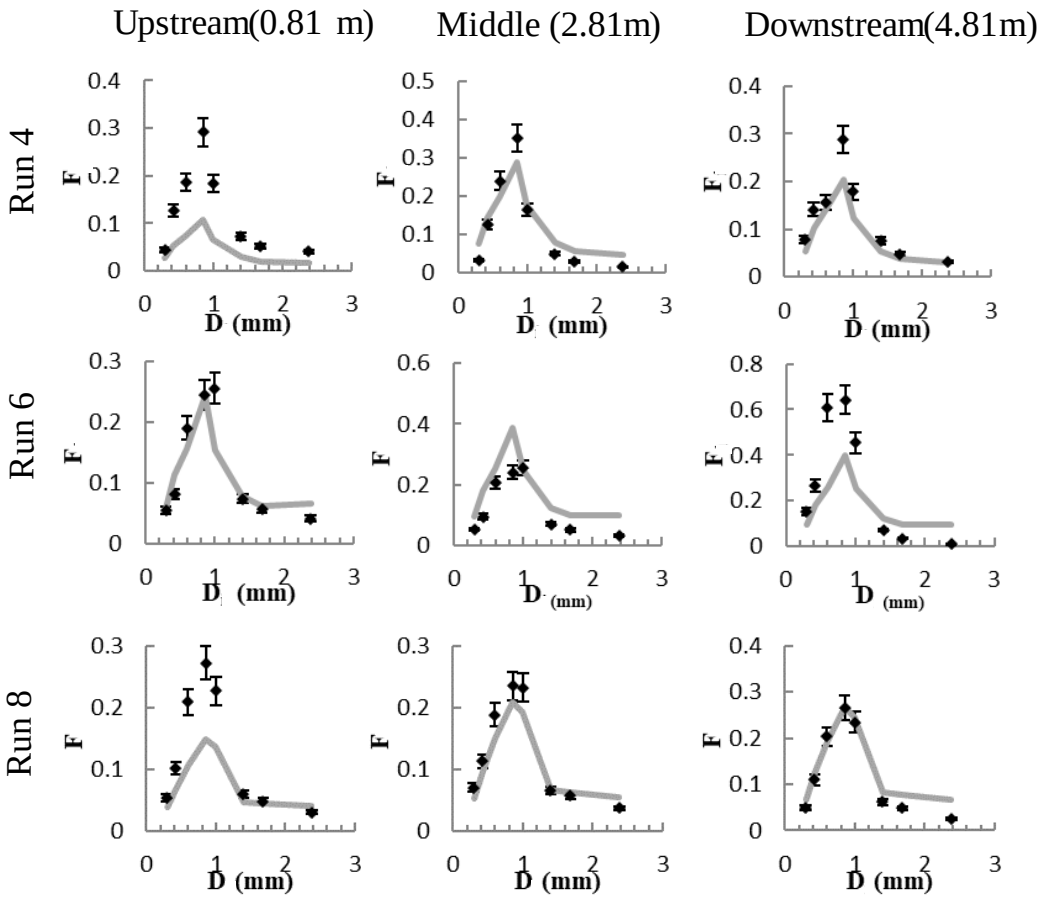

Figure 2.10 Comparison between measured and predicted grain size distributions of the bed surface sediment. The black dots are the experimental data and the continuous grey lines are the sediment size distributions predicted with the Ashida and Michiue bedload transport relation. The error bars indicate a 10 % error.

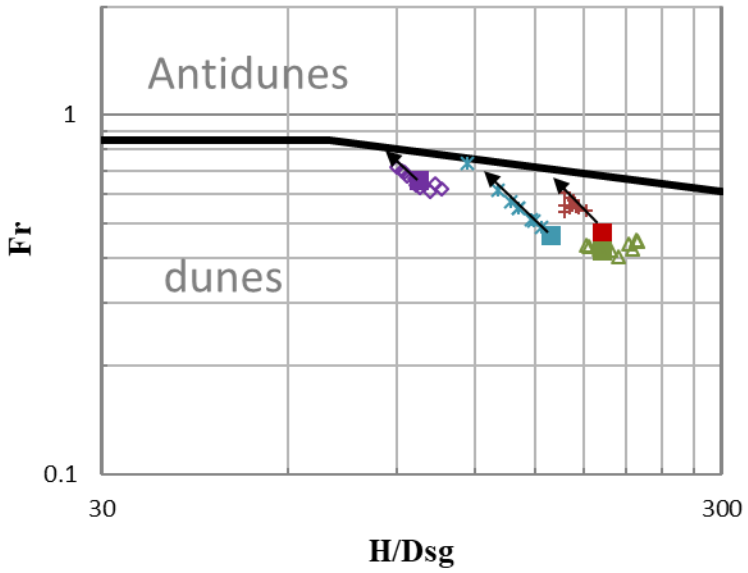

Figure 2.11 Vanoni (1975) diagram for bedform regime (grain size diameters of 0.93 mm, 1.20 mm, 1.35 mm). Blue stars are the points in Run 2, red pluses are the points in Run 4, green triangles are the points in Run 6 and the purple diamonds are the Run 8. Fully alluvial runs i.e., Runs 1, 3, 5 and 7 are respectively shown with blue, red, green and purple squares.

CHAPTER 3

MORPHODYNAMIC MODEL OF MIXED BEDROCK-ALLUVIAL REACHES CARRYING NON-UNIFORM BED MATERIAL

3.1 Introduction

Over the past decades numerous studies focused on the morphodynamics of mixed bedrock-alluvial rivers, in which a hardly erodible surface, the bedrock, interferes with in-channel sediment transport processes. Here I defined mixed bedrock-alluvial rivers as those with more than 5% of the channel bed composed of exposed bedrock and having the rest of the channel bed is covered with a relatively thin layer of alluvium (Howard, 1998). Mixed bedrock-alluvial reaches have been frequently observed in upland areas, where the bed material is relatively coarse and is preferentially transported as bedload and small scale bedforms such as dunes are generally absent (e.g. Whipple et al., 2000; Whipple and Tucker, 2002; Whipple, 2004; Sklar and Dietrich, 2004; Turowski et al., 2007; Gasparini et al., 2007; Chatanantavet and Parker, 2008, 2009; Lamb et al., 2008; Lague, 2010, 2014; Hodge et al., 2011, 2016; Chatanantavet et al., 2013; Johnson, 2014; Zhang et al., 2014; Inoue et al., 2014). Recent field studies demonstrated that mixed bedrock-alluvial rivers can also be found in lowland areas, where the bed material is relatively fine and small scale bedforms are present (Nittrouer et al., 2011; Shaw et al., 2013; Shaw and Mohrig, 2014).

It has long been thought that mixed bedrock-alluvial channels do not represent an equilibrium configuration of a river system. In other words, it was thought that they represent a transient condition in response to a change in hydrology or sediment supply or to a sudden change in base level (Howard, 1998). Equilibrium is a condition in which the bed elevation averaged over time scales that are long compared to the time scales of bedform migration (Blom et al., 2006) and bedload transport (Wong et al., 2007) is constant in time (Anderson et al., 1975). In the case of alluvial systems with constant base level, formative discharge and sediment supply, at equilibrium the bed material load is constant in space and in time and is equal to the sediment supply and to the transport capacity of the flow (e.g. Parker, 2004). Further, in alluvial systems at equlibrium the grain size distributions of the bed material load and of the bed surface are also constant in space and time if abrasion, tributaries, subsidence and sea level changes are not accounted for (Blom et al., 2016). In particular, the grain size distribution of the bed material load is equal to the grain size distribution of the sediment supply, while the grain size distribution of the bed surface sediment is generally coarser than the grain size distribution of the sediment supply to regulate the different mobility of coarse and fine grains (Blom et al., 2016).

Viparelli et al. (2015) demonstrated that low slope mixed bedrock-alluvial rivers might reach equilibrium conditions when the vertical distance between the bedrock surface and the water surface base level is small enough to influence in-channel sediment transport processes. It is important to note here than in the Viparelli et al. (2015) study equilibrium in mixed bedrock-alluvial rivers was obtained when bedrock incision, sea level rise and subsidence were not accounted for. One of the effects of bedrock incision, subsidence and sea level rise is to increase the vertical distance between the downstream water surface base

level and the bedrock surface. Thus, if these processes are accounted for, the mixed bedrock-alluvial river will tend to become alluvial as the vertical distance between the water surface base level and the bedrock surface increases in time.

Equilibrium in mixed bedrock-alluvial channels is characterized by steady but not uniform flow conditions, and the spatial changes in mean flow velocity are associated with spatial changes in the alluvial cover, i.e. the average fraction of the bed surface covered with alluvium (Viparelli et al., 2015). In particular, in the case of flow acceleration the alluvial cover decreases in the streamwise direction, and the opposite is observed in the case of spatial flow deceleration (Viparelli et al., 2015). The experiments presented in Chapter 2 of this dissertation showed that at equilibrium in mixed bedrock-alluvial rivers not only the alluvial cover fraction but also the flow resistances change in the flow direction. In particular, the experiments revealed that in the case of an equilibrium condition associated with a streamwise increase in flow velocity, the flow resistances decrease in the streamwise direction. This change in flow resistances is associated with downstream fining of the bed surface (reduction of skin friction), streamwise decrease in bedform height (reduction of form drag), or a combination of the two.

The downstream fining observed in the experiments can be explained recalling that in alluvial rivers at equilibrium the elevation of the bed deposit and the grain size distribution of the bed surface are constant in time. Thus, the total (i.e. summed over all the grain sizes) and the grain size specific bed material transport rates are equal to the transport capacity of the flow to guarantee mass conservation of bed material. In the case of mixed bedrock-alluvial rivers at equilibrium the flow is steady but not uniform, and thus the bed material transport capacity changes in space. The streamwise decrease in alluvial

cover limits the sediment availability so that the bed material load is everywhere equal to the sediment supply. Further, if the flow accelerates in the streamwise direction, as in the experiments of Chapter 2, a stable pattern of downstream fining may form in the mixed bedrock-alluvial reach. This pattern of downstream fining balances the increased transport capacity of the flow and the grain size distribution of the bed material load is everywhere equal to the grain size distribution of the sediment supply.

To the best of my knowledge, previous models of alluvial morphodynamics of mixed bedrock-alluvial systems did not account for the non-uniformity of the bed material and for the changes in flow resistances associated with a spatial change of the bedform geometry (Lague, 2010; Zhang et al., 2014; Johnson, 2014; Viparelli et al., 2015). Here I presented a one-dimensional formulation for the alluvial morphopdynamics of mixed bedrock-alluvial rivers that accounts for the non-uniformity of the bed material and the presence of small scale bedforms that influences flow resistances and sediment sorting patterns. I validated the numerical model with the experiments presented in Chapter 2, and then I applied the model to study the alluvial morphodynamics of a mixed bedrock-alluvial river with an equilibrium flow that decelerates in the downstream direction.

3.2 Model formulation

The model formulation is not site specific, i.e. the model can be applied to either field or laboratory scale and application-specific relations to compute the flow resistances and the bed material transport capacity must be chosen based on the characteristics of the problem. Model governing equations are the one-dimensional shallow water equations of mass and momentum conservation for open channel flow and the equation of conservation

of bed material. The following assumptions and approximations are introduced to simplify the problem:

1. The ratio between the volumetric bedload transport rate and the flow discharge is assumed to be orders of magnitude smaller than one so that the quasi-steady approximation holds for the flow (De Vries, 1965);

2. The bedrock is assumed to be non-erodible. The extension of the formulation to erodible bedrock surfaces is relatively straightforward (Lamb et al., 2008);

3. For the application at laboratory scale, a procedure to account for the different roughness between the smooth sidewalls and the rough bed is implemented (Vanoni and Brooks, 1957);

4. When applied at field scale the model describes the long-term evolution of the river channel. It does not account for the exchange of sediment between the river channel and the adjoining floodplain due to for example overbank deposition of suspended sediment, channel migration and widening (e.g. Viparelli et al., 2011; Lauer et al., 2016);

5. The base level is assumed constant, but the modification of the formulation to account for subsidence, uplift or sea level rise is straightforward (Viparelli et al., 2015);

6. Bed material is preferentially transported as bedload and thus suspended load can be neglected. The implementation of suspended load calculations is also relatively simple (Viparelli et al., 2015).

7. The cross section is assumed to be rectangular with uniform width that is not allowed to change in time. The extension of the present formulation to a spatially varying river cross section that does not change in time is cumbersome but not complex; and

8. The active layer approximation is used to model the exchange of bed material between the mobile bed and the bedload (Hirano, 1971; Parker, 1991a,b).

3.2.1 Model geometry

The schematic longitudinal profile of the modeled system is presented in Figure 3.1, where the black line represents the bedrock surface at elevation η_b, the grey line denotes the surface of the alluvial bed at elevation η and ζ is water surface elevation. The dashed line at elevation η_b+L_{ac} identifies the minimum elevation of the alluvial bed such that in-channel sediment transport processes are not affected by the underlying bedrock surface (Viparelli et al., 2015). In other words, L_{ac} represents the minimum thickness of the alluvial cover for complete channel bed alluviation. When the elevation of the alluvial bed η is smaller than η_b+L_{ac}, in-channel sediment transport processes are affected by the bedrock surface and the system is mixed bedrock-alluvial (Viparelli et al., 2015).

The location in which the elevation of the alluvial bed η is equal to η_b+L_{ac} separates a fully alluvial reach from a mixed bedrock-alluvial reach is indicated with a red circle in Figure 3.1. In Figure 3.1 the red circle separates an upstream alluvial reach from a downstream mixed bedrock-alluvial reach, i.e. it indicates the presence of an alluvial-bedrock transition (Viparelli et al., 2015). A bedrock-alluvial transition forms when the point with $\eta = \eta_b + L_{ac}$ separates an upstream mixed bedrock-alluvial reach from a downstream alluvial reach. An equilibrium alluvial-bedrock transition may form when S_b

< S_o and a bedrock-alluvial transition may form when $S_b > S_o$, with S_o denoting the equilibrium slope of an alluvial channel subject to the same flow regime and bed material load of the mixed bedrock-alluvial reach (Viparelli et al., 2015), and S_b being the slope of the bedrock surface.

3.2.2 Flow equations

The one-dimensional shallow water equations of mass and momentum conservation for open channel flow are presented in Equations (3-1) and (3-2) (Chaudhry, 2008).

$$\frac{\partial H}{\partial t} + \frac{\partial UH}{\partial x} = 0 \tag{3-1}$$

$$\frac{\partial U}{\partial t} + g\frac{\partial}{\partial x}\left(\frac{U^2}{2g} + H\right) = g\left(S - S_f\right) \tag{3-2}$$

where x and t respectively represent a streamwise and a temporal coordinate, U and H respectively denote the flow depth and the mean flow velocity, g is the acceleration of gravity, S is the channel bed slope defined herein as the slope of the alluvial bed, $S = -\partial h/\partial x$ and S_f denotes the friction slope. Equations (3-1) and (3-2) are simplified with the quasi-steady approximation (De Vries, 1975): the time derivatives in equations (3-1) and (3-2) are dropped and the equations of conservation of flow mass and momentum reduce to:

$$q_w = UH \tag{3-3}$$

$$g\frac{\partial}{\partial x}\left(\frac{U^2}{2g}+H\right)=g\left(S_o-S_f\right) \tag{3-4}$$

where q_w is the flow discharge per unit width. Substituting equation (3-3) into equation (3-4) the backwater equation for one-dimensional gradually varied steady flow is obtained

$$\frac{\partial H}{\partial x}=\frac{S-S_f}{1-Fr^2} \tag{3-5}$$

where Fr is the Froude number defined as $U/\sqrt{gH}$ and S_f represents the friction slope. Equation (3-5) is integrated in the upstream direction with the downstream boundary condition expressed in terms of known water surface base level, as appropriate in the case of subcritical flows. The friction slope S_f is defined as

$$S_f=\frac{C_f U^2}{gH} \tag{3-6}$$

where C_f is a non-dimensional friction coefficient. The calculation of C_f depends on the problem of interest. In the model validation runs presented below, I computed it as a function of the bed roughness with the *Manning-Strickler* formulation.

3.2.3 Equations of conservation of bed material

To account for the non-uniformity of the bed material grain size the sediment fluxes between the alluvial bed and the bed material load are modeled with the aid of the active layer approximation. In active layer-based models of alluvial systems, the deposit is divided in two regions, the active layer and the substrate. The active layer represents the topmost part of the deposit that interacts with the bed material load. It is modeled as a

mixed layer, i.e. its grain size distribution can change in the streamwise direction and in time but not in the vertical direction. The substrate is the part of the alluvial deposit underneath the active layer. The substrate grain size distribution can change in space, i.e. in the vertical and streamwise direction. Changes of the grain size distribution of the substrate in time can occur due to changes in the mean elevation of the deposit, i.e. the average elevation of the deposit averaged over a series of bedforms (Parker et al., 2000).

The definition of the active layer thickness L_a is not straightforward and relies on observations. In gravel bed rivers, where small scale bedforms such as dunes are generally absent (Parker and Klingemann, 1982), the active layer thickness scales with the coarsest grain sizes of the bed surface material. In sand bed rivers where small scale bedforms are generally present, the thickness of the active layer may scale with the bedform height (Viparelli et al., 2013). In the continuing of this section, I illustrated how the active layer approximation has been adapted to model the alluvial morphodynamics of a mixed bedrock-alluvial channel transporting non-uniform bed material.

In active layer-based models two equations of conservation of bed material are solved: the total, i.e. summed over all the grain sizes, equation of conservation of bed material to compute the changes in the mean elevation of the deposit, and the grain size specific equation of bed material to compute the streamwise and temporal changes of the grain size distribution of the active layer.

i. *Equation of conservation of bed material summed over all the grain sizes*

In mixed bedrock-alluvial rivers the equation of conservation of total bed material takes the following form (Zhang et al., 2015)

$$(1-\lambda_p)\,p_c\,\frac{\partial \eta}{\partial t} = -\frac{\partial q_{bT}}{\partial x} \tag{3-7}$$

where λ_p denotes the bulk porosity of the alluvial deposit, q_{bT} is the total volumetric bed material load per unit channel width and p_c represents the alluvial cover defined as the aerial fraction of the bed that is covered with alluvium (Nelson and Seminara, 2012; Inoue et al., 2014 and Johnson, 2014). Here p_c is modeled as in Viparelli et al. (2015) as

$$p_c = \begin{cases} 0.05 + 0.95\dfrac{\eta - \eta_b}{L_{ac}} & if \quad \dfrac{\eta - \eta_b}{L_{ac}} \le 1 \\ 1 & if \quad \dfrac{\eta - \eta_b}{L_{ac}} > 1 \end{cases} \tag{3-8}$$

with L_{ac} denoting the minimum thickness of alluvial cover for complete alluviation of the channel bed.

If the thickness of the alluvial deposit, $\eta - \eta_b$, is smaller than L_{ac}, exposed bedrock can be expected and $p_c < 1$. If the thickness of the alluvial deposit is larger than L_{ac}, the system is fully alluvial, and p_c is equal to 1. In the calculations presented below the total volumetric bed material load per unit channel width is equal to the total volumetric bed material transport capacity computed with an empirical relation, e.g. Ashida and Michiue (1972) or Wilcock and Crowe (2003), multiplied by the areal fraction of the channel bed covered with alluvium p_c.

ii. *Grain size specific equation of conservation of bed material*

In the case of bed material with uniform density, the one-dimensional, grain size specific conservation of bed material can be phrased as follows: the time rate of change of

the volume of bed material with characteristic grain size D_i in a control volume is equal to the net influx of bed material with grain size D_i in the control volume. In mixed bedrock-alluvial rivers the grain size specific equation of conservation of bed material in the case of constant bulk porosity of the deposit, λ_p, takes the form (see Zhang et al. (2015) for the derivation in the case of uniform sediment)

$$\left(1-\lambda_p\right)\frac{\partial}{\partial t}\int_{\eta_b}^{\eta} p_b f_i \, dz = -\frac{\partial q_{bi}}{\partial x} \tag{3-9}$$

where z denotes an upward oriented vertical coordinate, p_b represents the fraction of exposed bedrock at elevation z (Zhang et al., 2015), f_i is the volume fraction content of bed material with grain size D_i in the alluvial deposit and can vary in space (x and z) and in time, and q_{bi} is the bedload transport rate of bed material particles with characteristic grain size D_i. In the case of a fully alluvial system the lower limit of integration in equation (3-9) refers to a point very deep in the alluvial deposit (Parker et al., 2000), here the lower limit of integration corresponds to the elevation of bedrock surface. In analogy with the formulation illustrated above for the calculation of the total, i.e. summed over all the characteristic grain sizes, bed material load of sediment with characteristic grain size D_i, q_{bi} is equal to the product of the grain size specific transport capacity of bed material with characteristic grain size D_i and of the cover fraction p_c. The sum of the grain size specific bedload transport rates q_{bi} over all the grain size fractions is equal to the total bed material load q_{bT}.

The active layer approximation is used to solve the integral on the left-hand side of equation (3-9). If $\eta_b < \eta - L_a$ I expressed the integral as the sum of the integral of $p_b f_i$ in the

substrate, i.e. between η_b and η- L_a, and in the active layer, i.e. between η- L_a and η, with L_a denoting the active layer thickness in the case of a fully alluvial system. If $\eta_b > \eta - L_a$, the integral is equal to the product of p_b and the grain size distribution of active layer sediment.

Equation (3-10a) expresses the time rate of change of sediment with characteristic grain size D_i in a fully alluvial system, i.e. when $\eta_b < \eta - L_a$, Equation (3-10b) expresses the time rate of change of sediment with characteristic grain size D_i in a mixed bedrock-alluvial system, i.e. when $\eta_b > \eta - L_a$

$$\frac{\partial}{\partial t}\int_{h_b}^{h} p_b f_i \, dz = \frac{\partial}{\partial t}\left(\int_{h_b}^{h-L_a} p_b f_i' dz + \int_{h-L_a}^{h} p_b F_i \, dz \right) \tag{3-10a}$$

$$\frac{\partial}{\partial t}\int_{h_b}^{h} p_b f_i \, dz = \frac{\partial}{\partial t}\int_{h_b}^{h} p_b F_i \, dz \tag{3-10b}$$

where f_i' represents the volume fraction content of bed material with characteristic grain size D_i in the substrate, a function of z and x, and F_i is the volume fraction content of bed material with characteristic grain size D_i in the active layer, i.e. a function of x and time.

Recalling that in the present formulation I neglected bedrock incision, subsidence and uplift, the limit of integration that are a function of time are η and L_a. Thus, the Leibnitz rule is applied to solve the first integral on the right-hand side of equation (3-10a) expressing the grain size specific fluxes of sediment between the active layer and the substrate associated with changes in the elevation of the active layer – substrate interface

$$\frac{\partial}{\partial t}\int_{h_b}^{h-L_a} p_b f_i' dz = \int_{h_b}^{h-L_a} \frac{\partial\left(p_b f_i'\right)}{\partial t} dz + \left(p_b f_i'\right)\Big|_{z=h-L_a} \frac{\P}{\P t}\left(h - L_a\right) = p_{bI} f_{Ii} \frac{\P}{\P t}\left(h - L_a\right) \tag{3-11}$$

where f_{Ii} denotes the volume fraction content of bed material with grain size D_i at the active layer-substrate interface and p_{bI} the alluvial cover at the active layer-substrate interface.

The second integral on the right hand side of equation (3-10b) expressing the grain size specific conservation of bed material in the active layer can be solved recalling that F_i is not functions of z, and that the integral of p_b between the active layer-substrate interface represents the volume of sediment between elevations $\eta - L_a$ and η, i.e. the average thickness of the active layer $L_{a,av}$. In a fully alluvial system $p_b = 1$, $L_{a,av} = L_a$ and the integral is equal to the time rate of change of $F_i L_a$. In mixed alluvial-bedrock reaches, due to the presence of exposed bedrock $L_{a,av} < L_a$. Similarly, the integral in Equation (3-10b) is equal to $F_i L_{a,av}$. Combining equations (3-9) - (3-11), the grain size specific equation of bed material takes the form

$$(1-l_p)\left[p_{bI} f_{Ii} \frac{\partial}{\partial t}(h - L_a) + \frac{\partial}{\partial t}(F_i L_{a,av})\right] = -\frac{\partial q_{bi}}{\partial x} \tag{3-12}$$

When $\eta_b > \eta - L_a$ the first term in the left-hand side of equation (3-12) representing the sediment fluxes between the active layer and the substrate is equal to zero. When the elevation of the active layer-substrate interface is higher than the elevation of the bedrock surface ($\eta_b < \eta - L_a$), the volume fraction content of bed material at the active layer-substrate interface, f_{Ii}, is computed with the formulation proposed by Hoey and Ferguson (1994), as

$$f_{Ii} = \begin{cases} f_i'\Big|_{z=h-L_a}, & \dfrac{\partial h}{\partial t} < 0 \\ \alpha F_i + (1-\alpha) f_{load,i}, & \dfrac{\partial h}{\partial t} \geq 0 \end{cases} \tag{3-13}$$

where $0 < \alpha < 1$ and $f_{load,i}$ is the volume fraction content of bed material in the generic grain size range in bedload transport, which is equal to q_{bi}/q_{bT}.

As in the Zhang et al. (2015) formulation the fraction of exposed bedrock at elevation z, p_b, can vary in the streamwise direction and in time. It is, however, necessary to specify a function to compute p_b and solve the problem. Here, following Zhang et al. (2015) and Viparelli et al. (2015) I defined the thickness of the alluvial cover, p_c, as the vertical distance between the locally averaged elevation of the alluvium, η, and the elevation of the bedrock surface η_b. Thus, $p_b(z = \eta) = p_c(\eta)$ and I used equation (3-8) to determine $L_{a,av}$ and p_{bI} in equation (3-12).

3.2.4 Flow resistances calculations

In alluvial rivers the flow resistances are generally associated with the presence of a granular bed (skin friction) and with the presence of bedforms (form drag), and the channel bed irregularities are modeled in terms of a roughness height that in the case of skin friction scales with the bed material grain size (e.g. Parker, 2004). In mixed bedrock-alluvial rivers part of the flow resistances are also associated with the irregularities of the exposed bedrock surface.

Johnson (2014) proposed a model to determine the friction coefficient in mixed bedrock-alluvial rivers that accounts for flow resistances associated with the alluvial patches and the exposed bedrock on the channel bed. In particular, Johnson (2014) defined

an equivalent friction coefficient for mixed bedrock-alluvial rivers equal to the weighted average over the alluvial cover of the friction coefficients of the areas covered with alluvium and of the exposed bedrock. To estimate the equivalent friction coefficient Johnson (2014) considered 1) the grain roughness in the alluvial parts of the river bed, 2) the macro roughness of the alluvial bed fluctuations and 3) the macro roughness associated with bedrock surface fluctuations. Here I also considered the case in which the macro roughness of the alluvial bed fluctuations is associated with small scale bedforms such as dunes, which significantly contribute to the flow resistances.

In particular, I estimated the friction coefficient of the mixed bedrock-alluvial reach, C_f, with the Manning-Strickler formulation (equation 3-14).

$$C_f^{-1/2} = \alpha_r \left(\frac{R_h}{k_t}\right)^{1/6} \tag{3-14}$$

where α_r is a constant equal to 8.1 in the present study (Parker, 1991), R_h denotes the hydraulic radius of the bed region and k_t represents an equivalent bed roughness height. More details on the empirical relations for calculation of flow resistances are presented in section 3.3.1

3.3 Empirical relations to validate the model at laboratory scale

The numerical framework presented above is validated against the laboratory experiments presented in Chapter 2. In this section I described the empirical relations used to model the laboratory experiments and the comparison between numerical and experimental results is presented in section 3.4. The experiments presented in Chapter 2

were performed either with relatively well sorted sand or with poorly sorted sand and were specifically designed to investigate the equilibrium of mixed bedrock-alluvial channels. The experiments were conducted in a sediment feed flume and the results of the runs with a mixed bedrock-alluvial reach were compared with the results of alluvial equilibrium experiments performed with the same feed rates and flow rates of mixed bedrock-alluvial experiments.

In these experiments the model bedrock was a sheet of marine plywood glued on the bottom of the flume. The roughness of the bedrock surface was modeled with uniform sand grains of ~1 mm in diameter glued to the model bedrock. The experiments were performed with constant feed rate, flow rate and water surface base level. The grain size distribution of the sediments used in the experiments is presented in Figure 2.2 of chapter 2, in which the black line is the grain size distribution of the uniform sand with the geometric mean diameter D_g = 1.11 mm and the geometric standard deviation σ_g = 1.44 and the grey line is the grain size distribution of the nonuniform sand with the geometric mean diameter D_g = 0.87 mm and the geometric standard deviation σ_g = 1.69.

When the flow and the bedload transport system reached a condition of mobile bed equilibrium, the average bed and water surface elevation were measured and the cover fraction and the flow characteristics averaged over a series of bedforms were computed, as illustrated in Chapter 2. The measurements of bed elevation provided information on the spatial variability of bedform geometry in the mixed bedrock-alluvial reach. At the end of the experiments surface sediment samples were collected to measure the grain size distribution of the bed surface, defined as the entire thickness of the alluvial layer in the mixed bedrock-alluvial reaches.

3.3.1 Empirical relation to compute the flow resistances.

The experiments presented in Chapter 2 were performed in a 0.19 cm wide laboratory flume, thus for a proper calculation of the flow resistances and of the shear stresses acting on the channel bed the different roughness between the rough bed and the smooth flume sidewalls must be accounted for (Vanoni and Brooks, 1957). I thus implemented the Vanoni and Brooks (1957) sidewall correction procedure as described in Chiew and Parker (1994) to estimate flow resistances and bed shear stress from laboratory data collected in narrow flumes, with the formulation illustrated in Chapter 2

Noting that during the experiments dunes formed and migrated downstream, the sidewall corrected bed shear stresses accounted for different types of flow resistances, the flow resistances associated with the presence of a granular bed (skin friction), the flow resistances associated with the presence of bedforms (form drag) and the flow resistances associated with the presence of the model bedrock. The form drag does not contribute to bedload transport (e.g. Engelund and Hansen, 1967) and thus the bed shear stresses associated with skin friction must be computed for the bedload transport calculation. The procedure followed to partition the flow resistances associated with skin friction and form drag (Einstein decomposition) is presented in Appendix. For the calculation of the flow resistances with equations (3-14) I needed to determine the composite friction coefficient of the alluvial parts and of the exposed bedrock which takes the following form (Johnson, 2014)

$$C_{fb} = p_c C_{fb,a} + (1 - p_c) C_{fb,b} \tag{3-15}$$

Where C_{fb} denotes the total friction coefficient for the bed region which is computed with the Vanoni and Brook (1957) procedure, $C_{fb,a}$ is the bed friction coefficient for the alluvium and $C_{fb,b}$ is the bed friction coefficient for the exposed bedrock. Equations (3-16a and b) are the friction coefficient for the alluvium and for the bed region respectively. Using a Manning-Strickler formulation the friction coefficients for the alluvial and the bed regions can be respectively computed as (Parker, 2004)

$$C_{fb,a}^{-1/2} = \alpha_r \left(\frac{R_{hb,a}}{k_c}\right)^{1/6} \tag{3-16a}$$

$$C_{fb,b}^{-1/2} = \alpha_r \left(\frac{R_{hb,b}}{k_{sbr}}\right)^{1/6} \tag{3-16b}$$

where $R_{hb,a}$ is the hydraulic radius associated with the alluvium, k_c denotes the roughness height of the alluvium including both form drag and skin friction, $R_{hb,b}$ is the hydraulic radius associated with the exposed bedrock and the k_{sbr} represents the roughness height of the bedrock which is 1 mm in the present study. $R_{hb,b}$ is computed from manning formulation as follows

$$R_{hb,b} = \left(\frac{U k_{sbr}}{\alpha_r \sqrt{g} S_f^{1/2}}\right)^{3/2} \tag{3-17}$$

where S_f is the friction slope. Using equations (3-15, 3-16b and 3-17) I could compute $C_{fb,a}$. Thus in equation 3-16a, I had two unknowns which are $R_{hb,a}$ and k_c . Assuming that the friction slope is the same in both alluvium and exposed bedrock, which is equal to the

friction slope of the entire cross section (Vanoni and Brooks, 1957), the following relation linking friction coefficients and hydraulic radius is found.

$$\frac{C_{fb}}{R_{hb}} = \frac{C_{fb,a}}{R_{hb,a}} \tag{3-18}$$

Using equation 3-18 and 3-16a, I could compute the hydraulic radius and the composite roughness for the alluvium and for the bed region. After obtaining the friction coefficient for the alluvium, I could follow the procedure presented in Appendix A (Einstein decomposition) to partition the alluvial resistances between the flow resistances associated with skin friction and form drag. The friction coefficient associated with skin friction is then used to compute the bedload transport.

3.3.2 Bedload transport formulation

The comparison between grain size specific bedload transport rates measured during the experiments described in Chapter 2 and those predicted with the surface-based version of the Ashida and Michiue (1972) bedload transport relation demonstrated that the Ashida and Michiue formulation is able to reasonably reproduce the total and grain size specific sediment fluxes in the experiments with exposed bedrock (Figures 2.9 and 2.10 of Chapter 2). Thus, in the model validation presented below I implemented the Ashida and Michiue bedload transport model to compute the grain size specific sediment fluxes.

The Ashida and Michiue (1972) bedload relation for mixtures of sediment particles differing in size takes the form

$$q_{bi}^{*} = 17\left(\tau_{bsi}^{*} - \tau_{refi}^{*}\right)\left(\sqrt{\tau_{bsi}^{*}} - \sqrt{\tau_{refi}^{*}}\right) \tag{3-19}$$

where the subscript i refers to the grain size range with characteristic grain size D_i, q_{bi}^{*} is the grain size specific Einstein number, i.e. the non-dimensional volumetric bed material load per unit channel width, τ_{bsi}^{*} is the grain size specific Shields number associated with skin friction, i.e. the non-dimensional bed shear stress associated with skin friction, and τ_{refi}^{*} is the grain size specific reference Shields number for the initiation of significant bedload transport of particles with characteristic grain size D_i (Parker, 2008).

The grain size specific Einstein number and the grain size specific Shields number associated with skin friction are respectively defined in Equations (3-20) and (3-21)

$$q_{bi}^{*} = \frac{q_{bi}}{\sqrt{RgD_i}\, D_i\, p_c F_i} \tag{3-20}$$

$$\tau_{si}^{*} = \frac{\tau_s}{\rho R g D_i} \tag{3-21}$$

where R denotes submerged specific gravity of the sediment, g represents the acceleration of gravity. τ_s is the bed shear stress associated with skin friction and ρ denotes the water density.

The grain size specific reference value of the Shields number of Equation (3-19) is computed with the following hiding/exposure function

$$\frac{\tau^*_{refi}}{\tau^*_{srg}} = \begin{cases} 0.843\left(\frac{D_i}{D_{sg}}\right)^{-1} & for \frac{D_i}{D_{sg}} \le 0.4 \\ \left[\frac{log(19)}{log\left(19\frac{D_i}{D_{sg}}\right)}\right]^2 & for \frac{D_i}{D_{sg}} > 0.4 \end{cases} \quad (3\text{-}22)$$

where τ^*_{srg} is a reference value equal to 0.05 and D_{sg} represents the geometric mean diameter of the bed surface sediment (Parker, 2008).

3.3.3 Definition of the minimum thickness of alluvial cover

In the experiments presented in Chapter 2 the exposed bedrock appeared downstream of the lee faces of the dunes and the bed elevation measurements showed that one of the results of the interaction between the bedform and the underlying non-erodible surface was a reduction of the bedform height compared to fully alluvial experiments performed with the same sediment feed rate and flow discharge, the formation of a stable pattern of downstream fining in the mixed bedrock-alluvial reaches, or a combination of the two. Further, Tuijnder et al. (2009) performed experiments on sand dunes migrating on an immobile gravel layer and showed that the interaction between the gravel layer and the bedforms became negligible when the average thickness of the alluvial layer was equal or greater than ~1.5 times the bedform height.

Based on these experimental observations I set the minimum thickness of alluvial cover for complete alluviation L_{ac} to be 1.5 times the standard deviation of the bed

elevation fluctuations which is a representative for bedform height, as discussed in Chapter 2. Noting that the formulation presented in Equation (3-8) has not been validated against any experimental observation or field data, I compared the alluvial cover p_c predicted with equation (3-8) with the experimental measurements. The comparison is presented in Figure 3.2, where the grey dots represent the experimental measurements, the straight line represents equation (3-8) and the dashed lines represent a 25% difference between measurements and predictions. Noting that the difference between measurements and predictions is larger than 25% in only 3 cases corresponding to ~10% of the experimental points, I concluded that equation (3-7) can be reasonably used to predict the alluvial cover fraction to perform one-dimensional, i.e. laterally averaged, simulations of the experiments and can thus be used for model validation.

3.3.4 Active layer thickness

For the validation of the numerical model, I assumed that the active layer thickness for the fully alluvial runs L_a is equal the standard deviation of the bed elevation measurements in the fully alluvial runs. Noting that active layer-based models cannot capture the fine details associated with bedform migration, I assumed that one standard deviation of bed elevation fluctuation is a reasonable measure of the average thickness of the layer that exchanges sediment with the bedload transport. In the calculations presented herein the standard deviation of bed elevation at equilibrium in the fully alluvial runs made non-dimensional with the geometric mean diameter of the bed surface is computed as a function of the Froude number of the flow. The comparison between experimental measurements and the proposed relation is presented in Figure 3.3. The data in Figure 3.3

show that in the experiments the non-dimensional standard deviation of bed elevation decreases with increasing Froude numbers, i.e. the dune height decreases as the Froude number increases and the flow regime tends towards the upper regime (Chapter 2).

3.3.5 The flow of the calculation

The modeled domain is divided into N reaches bounded by N+1 computational nodes. The model initial conditions are specified in terms of a longitudinal profile of alluvial bed elevation averaged over a series of bedforms and the bed surface grain size distribution. The model boundary conditions are assigned in terms of a longitudinal profile of bedrock elevation, flow rate, sediment feed rate and sediment size distribution, and downstream water surface base level. The flow equation (3-5) is integrated in the upstream direction. The bed shear stresses are then estimated in each computational node, and the sidewall correction and Einstein decomposition have been applied to the model to compute the shear stresses associated with skin friction. The bedload transport rate is computed with the surface-based version of the Ashida and Michiue (1972) formulation modified to account for the presence of exposed bedrock (Viparelli et al., 2015) i.e. equations (3-19, 3-22). The equation of conservation of total bed material (equation 3-7) is then solved to estimate the time rate of change of mean alluvial bed elevation and finally the grain size specific equation of conservation of active layer sediment (equation 3-12) is solved to update the grain size distribution of the bed surface. Given the new longitudinal profile of alluvial bed elevation and the grain size distribution of the bed surface, the calculations are repeated until the system reached equilibrium condition i.e. conditions in which the bed elevation averaged over a series of bedforms does not change in time and the bedload transport rate becomes equal to the upstream sediment supply in each node. In preparation

for future field scale applications, the model has been implemented to end the calculations when a user specified time period has been simulated.

3.4 Model validation at laboratory scale

The flow rates in the experiments presented in Chapter 2 and used for the model validation at laboratory scale varied between 10 and 20 l/s and the feed rates ranged between 700 gr/min and 400 gr/min. The model validation was performed in two phases: equilibrium model results were first compared against the alluvial equilibrium experiments to verify that the present formulation can reproduce the equilibrium characteristics of a fully alluvial system. The second phase of the model validation consisted in the comparison between experimental measurements and numerical predictions of the equilibrium in the experiments with mixed bedrock-alluvial reaches. The model boundary conditions for the validation runs are presented in Table 2.1 in chapter 2 in terms of flow rate, sediment feed rate, sediment type (uniform or non-uniform sand), and downstream water surface base level.

It is important to note here that the empirical relations used for the model validation presented in section 3 and in Figure 2.9 of Chapter 2 show a reasonable agreement between predicted and measured equilibrium values. Thus, in the model validation presented herein significant differences between numerical predictions and experimental measurements cannot depend on the empirical relations and, if they appear, they identify weaknesses and limitations of the formulation for the alluvial morphodynamics of mixed bedrock-alluvial rivers transporting non-uniform bed material.

3.4.1 Alluvial equilibrium runs

The comparisons between measured and modeled alluvial equilibrium values of equilibrium water depth, bed slope, bed shear stress associated with skin friction and the geometric mean diameter of the surface material are respectively presented in Figures 3.4a-d. In the plots of Figure 3.4 the numerical equilibrium values are on the horizontal axes and the measured values are on the vertical axes. The continuous black lines denote the perfect agreement between numerical predictions and experimental observations. Each black diamond represents one alluvial equilibrium experiment (Table 2.1). The dashed grey lines represent error bounds around the line of perfect agreement. Numerical predictions of water depth, and thus flow velocity (Equation 3-3), are within 10% error from the experimental observations. Numerical predictions of bed slopes are within 30% error of the measured value. The comparison between numerical and experimental predictions of shear stress associated with skin friction and geometric mean diameter of the surface material respectively are within 30% and 10% error. The comparison between numerical predictions and experimental observations presented in Figure 3.4 shows that, given the model simplifications and the use of empirical relations to compute the flow resistances and the sediment fluxes, the proposed model is able to capture the experimental observations with errors that are comparable with those of other one-dimensional, active layer-based models of alluvial morphodynamics (e.g. Viparelli et al., 2010; Viparelli et al., 2014).

3.4.2 Equilibrium runs with a mixed bedrock-alluvial reach

The comparison between the numerical predictions and the experimental measurements is presented in Figure 3.5 in terms of water surface and bed elevations in Figures 3.5 (panels a, c, f and i); alluvial cover in Figures 3.5 (panels b, d, g, and j); and geometric mean diameter of the bed surface sediment in Figures 3.5 (panels e, h and k). The comparison between numerical and experimental results for the runs with uniform sand are presented in Figures 3.5 (panels a and b) i.e. Run 2. The comparisons between numerical and experimental results for the runs with non-uniform bed material are in Figures 3.5 (panels c-k). In particular, the comparison for Run 4 is in Figures 3.5 (panels c-e), the comparison for Run 6 is in Figures 3.5 (panels f-h), and the comparison for Run 8 is in Figures 3.5 (panels i-k).

In Figures 3.5 (panels a, c, f and i) the black diamonds and the grey triangles respectively represent measured values of water surface and alluvial bed elevation above the bedrock. The continuous black line represents the numerical predictions of water surface elevation, and the continuous grey lines are the numerical results of equilibrium bed elevation. The error bars denote 10% error for the water surface elevation and 20% error for bed surface elevation. The modeled equilibrium bed and water surface elevations are in reasonable agreement with the experimental results in the mixed bedrock-alluvial reaches (error smaller than 20%). The relatively large differences between numerical predictions and experimental data in the alluvial reach in the upstream part of the modeled domain are due to the empirical model for the calculation of the flow resistances. The length of the alluvial reaches in the runs with exposed bedrock was chosen to be of comparable length with the bedform development region, i.e. the region in which the bedform grew and formed in the experimental runs. Noting that the relation to compute

the standard deviation of bed elevation proposed in Figure 3.2 is based on equilibrium values, i.e. values in which the bedforms are fully developed and thus larger than those observed in the experiments, the model predicts flow resistances and water depths that are larger than those measured in the experiments. Consequently, the predicted bed shear stresses associated with skin friction and the bed material transport capacities predicted with equations (3-20) and (3-21) are larger than those observed in the experimental runs, and the numerical equilibrium bed slopes of the alluvial reaches are milder than those measured during the experiments.

The comparison between numerical and predicted alluvial cover is presented in Figures 3.5 (panels b, d, g and j) in which the black diamonds represent the experimental points and the continuous lines are the corresponding numerical simulations. The alluvial cover is unity where the reach is entirely covered with sediment (fully alluvial) and is less than unity where the cross section is partially covered with sediment (mixed bedrock-alluvial). The alluvial cover plots show that the model can reasonably capture the position of the alluvial-bedrock transition. The sudden drop in the alluvial cover measured in the experiments is not reproduced in the numerical simulations. In the mixed bedrock-alluvial reaches the model can reproduce the observed rates of alluvial cover reduction in the streamwise direction. In other words, the slope of the line indicating the numerical model results is nearly parallel to the regression line through the experimental points in the mixed bedrock-alluvial reaches.

The difference between numerical predictions of cover fraction and the experimental results near the alluvial-bedrock transitions is associated with small scale phenomena that cannot be captured with an active layer model, i.e. the flow separation on

the downstream side of the bedforms and that caused a rapid increase in exposed bedrock downstream of the lee faces.

The comparison between predicted and measured geometric mean diameters of the equilibrium bed surface material are presented in Figures 3.5 (panels e, h and k). The black diamonds represent the experimental points and the lines are the numerical model prediction. The bars indicate the 5 % error and most of the points fall within these error bars (except 2 points in the run 6 and 2 points in the run 8) suggesting a remarkably good agreement between numerical and predicted grain size distributions of the bed surface sediment.

The comparison between numerical and measured grain size distribution (GSD) of the surface material is presented in Figure 3.6 for samples collected at 0.81 m, 2.81 m and 4.81 m from the test reach entrance. In this figure the black diamonds denote the experimental grain sizes, the line is the model prediction and the bars indicate the 10 % error in the plots. The comparison for Run 4 (flow rate of 20 l/s and feed rate of 700 gr/min) is presented in Figures 3.6 (panels a-c); Figures 3.6 (panels d-f) present the comparison between numerical and experimental results for Run 6 (flow rate of 20 l/s and feed rate of 400 gr/min); and the numerical and experimental results for Run 8 (flow rate of 10/s and feed rate of 400 gr/min) are in Figure 3.6 (panels g-i). The panels of Figure 3.6 confirm that the proposed model is able to predict the grain size distribution of the equilibrium bed surface (and thus the bed material fluxes) with errors that are comparable (if not smaller) with those of one-dimensional models of alluvial morphodynamics (e.g. Viparelli et al., 2010; Viparelli et al., 2014).

3.5 Discussion

The validated model is used herein to study changes in flow resistances and the associated sediment sorting patterns in bedrock reaches that for upstream of a stable bedrock-alluvial transition, i.e. a transition from a mixed bedrock-alluvial reach to an alluvial reach that forms when the slope of the bedrock surface S_b is larger than the equilibrium slope of a river reach subject to the same flow regime and sediment supply. Figure 3.7 schematically shows how a mixed bedrock-alluvial reach forms upstream of a bedrock-alluvial transition. The black line shows the bedrock surface, the grey line denotes the bed surface elevation, the blue line represents the water surface elevation and the dashed grey line represents the minimum thickness for complete alluviation.

For these simulations I used the experimental conditions of Run 4, i.e. non-uniform sand, feed rate equal to 700 gr/min and flow rate equal to 20 l/s. The numerical results are presented in Figure 3.8, in which the panel (a) shows the equilibrium alluvial bed surface elevation (orange line) and the bedrock elevation (black line). The dashed grey line identifies the minimum thickness of alluvial cover for the complete alluviation of the channel bed, the red circle and the dashed green line identify the equilibrium position of the stable bedrock-alluvial transition. The spatial changes in water depth at equilibrium are presented in Figure 3.8 panel (b), in which the blue line denotes the water depth and the dashed green line identifies the position of the bedrock-alluvial transition. In the bedrock reach upstream of the bedrock-alluvial transition the flow depth increases in the flow direction until it reaches the alluvial equilibrium value H_o at the bedrock-alluvial transition. The water depth remains constant in space and equal to H_o over the alluvial reach.

The spatial increase in flow depth presented in Figure 3.8 panel (b) is associated with a spatial decrease in mean flow velocity and bedload transport capacity of the flow. Recalling that at equilibrium the bedload transport rate is equal to the sediment supply, a spatial decrease of the bedload transport capacity has to be associated with an increase of the alluvial cover fraction *pc*, equation (3-20). The predicted streamwise increase of the alluvial cover fraction in the mixed bedrock-alluvial reach is presented in Figure 3.8 panel (c), where the dashed green line identifies the location of the bedrock-alluvial transition. In the alluvial reach $p_c = 1$ and the bedload transport rate is everywhere equal to the bedload transport capacity and to the sediment supply. Finally, the spatial variation of the geometric mean diameter of the bed surface sediment, D_{sg}, is presented in Figure 3.8 panel (d). In the equilibrium alluvial reach D_{sg} does not vary in space. In the mixed bedrock-alluvial reach it increases in the flow direction until it reaches its alluvial equilibrium value at the bedrock-alluvial transition. The coarsening of the bed surface sediment in the mixed bedrock-alluvial reach can be explained considering that, due to the spatial deceleration of the flow, the bed material transport capacity decreases in the flow direction. As the bed material transport capacity decreases in the flow direction, the mobility of the coarse grains significantly decreases compared to the mobility of the fine grains, and thus their volume fraction content on the bed surface, F_i, has to increase to ensure the sediment mass conservation, equation (3-20).

The numerical results presented in Figure 3.8 show that when the slope of the bedrock surface is steeper than the alluvial equilibrium slope of a fluvial reach subjected to the same flow and sediment supply, the flow characteristics on the mixed bedrock-alluvial reach tend to be associated with a spatial deceleration of the flow associated with

a streamwise increase of the alluvial cover and the formation of a pattern of downstream coarsening of the bed surface sediment. Conversely, when the slope of the bedrock surface is milder than the alluvial equilibrium slope of a river reach subjected to the same flow regime and sediment supply (experiments of chapter 2), the flow hydrodynamics in the mixed bedrock-alluvial reach is characterized by a spatial acceleration of the flow in the streamwise direction associated with a reduction of alluvial cover and the formation of a pattern of downstream fining of the bed surface sediment.

Due to the lack of predictive models describing the changes in bedform regime and bedform size in mixed bedrock-alluvial reaches, the spatial changes in bedform geometry have not been predicted with the simulations. Based on the experimental observations presented in Chapter 2, I hypothesized that depending on the characteristics of the alluvial equilibrium bedforms, the bedform height in mixed bedrock-alluvial reaches upstream of a stable bedrock-alluvial transition may increase in the streamwise direction in the case of lower regime bedforms. In other words, the experiments presented in Chapter 2 suggested that in the case of spatial flow acceleration the bedform regime tend to move from dunes to antidunes with a reduction of the flow resistances associated with form drag. In the case of the spatial flow deceleration observed upstream of a stable bedrock-alluvial transition, I expected to see an increase in dune height associated with an increase in flow depth, reduction in mean flow velocity and increasing flow resistances associated with form drag.

3.6 Conclusions

I presented a novel one-dimensional mathematical formulation for the alluvial morphodynamics of mixed bedrock-alluvial rivers that explicitly accounts for the non-

uniformity of the sediment size and the different roughness between the exposed bedrock and the alluvial patches. The alluvial flow resistances are further partitioned between skin friction and form drag to properly estimate the sediment transport rates.

The formulation, implemented in a numerical model, has been validated against the experimental results presented in Chapter 2. The differences between the numerical predictions and the experimental observations in the mixed bedrock-alluvial reaches are comparable with the differences between numerical and experimental values presented in similar studies on the alluvial morphodynamics of fluvial reaches.

The model validation was performed in the case of an equilibrium mixed bedrock-alluvial reach that formed downstream of an alluvial-bedrock transition, which may form if the bedrock surface slope is smaller than the alluvial equilibrium slope of an alluvial reach subjected to the same flow regime and sediment supply. This equilibrium case is characterized by spatial flow acceleration on the mixed bedrock-alluvial reach associated with a streamwise decrease of the alluvial cover, fining of the bed surface sediment and reduction of dune height.

The application of the model to study the alluvial morphodynamics of mixed bedrock-alluvial reaches that form upstream of a stable bedrock-alluvial transition, which may form when the slope of the bedrock surface is larger than the slope of an alluvial reach subjected to the same flow regime and sediment supply, reveals that the equilibrium flow hydrodynamics of the mixed bedrock-alluvial reach is characterized by flow deceleration in the downstream direction. The numerical simulations show that this flow deceleration is associated with a streamwise increase of the alluvial cover fraction and the formation of

a stable pattern of downstream coarsening of the bed surface sediment to balance the reduction of the bedload transport capacity. Based on the experimental observations of Chapter 2, I hypothesized that if dunes form on the alluvial reach, the bedform height in the mixed bedrock-alluvial reach should increase in the flow direction.

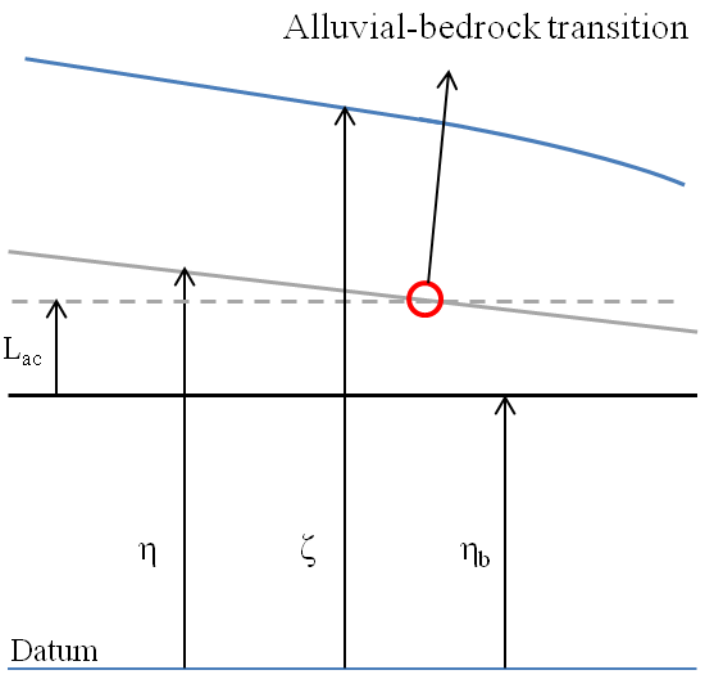

Figure 3.1 Schematic geometry of the modeled domain. Flow goes from left to right. Black solid line is the bedrock surface. The grey line is the bed surface and blue thick line represents the water surface. The red circle is showing the alluvial-bedrock transition.

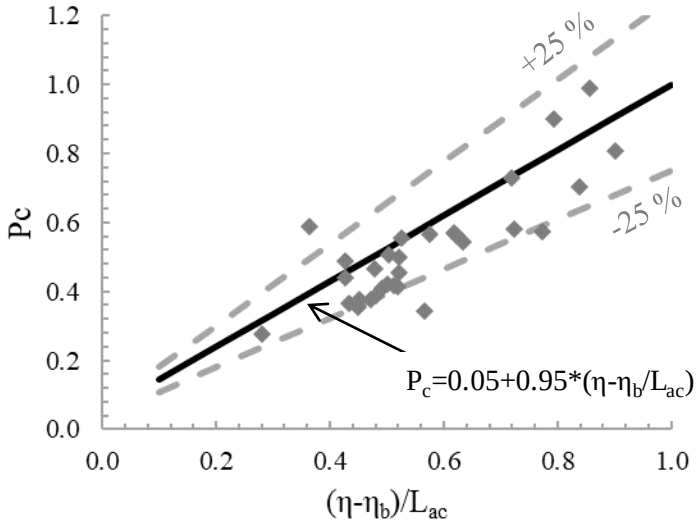

Figure 3.2 Alluvial cover fraction formulation of Viparelli et al. 2015 vs experimental data.

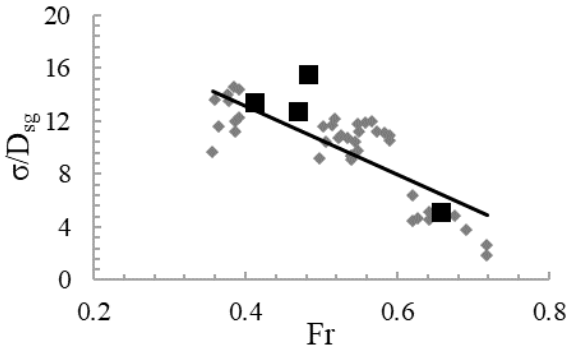

Figure 3.3 Flow resistance analysis of the experimental data. Dimensionless standard deviation of the bed elevation fluctuation Vs Froude number. Grey diamonds represent the mixed bedrock-alluvial points and black squares are the fully alluvial runs. The black line represents the linear regression to mixed bedrock-alluvial points ($\sigma/D_{sg} = -25.97Fr + 23.50$)

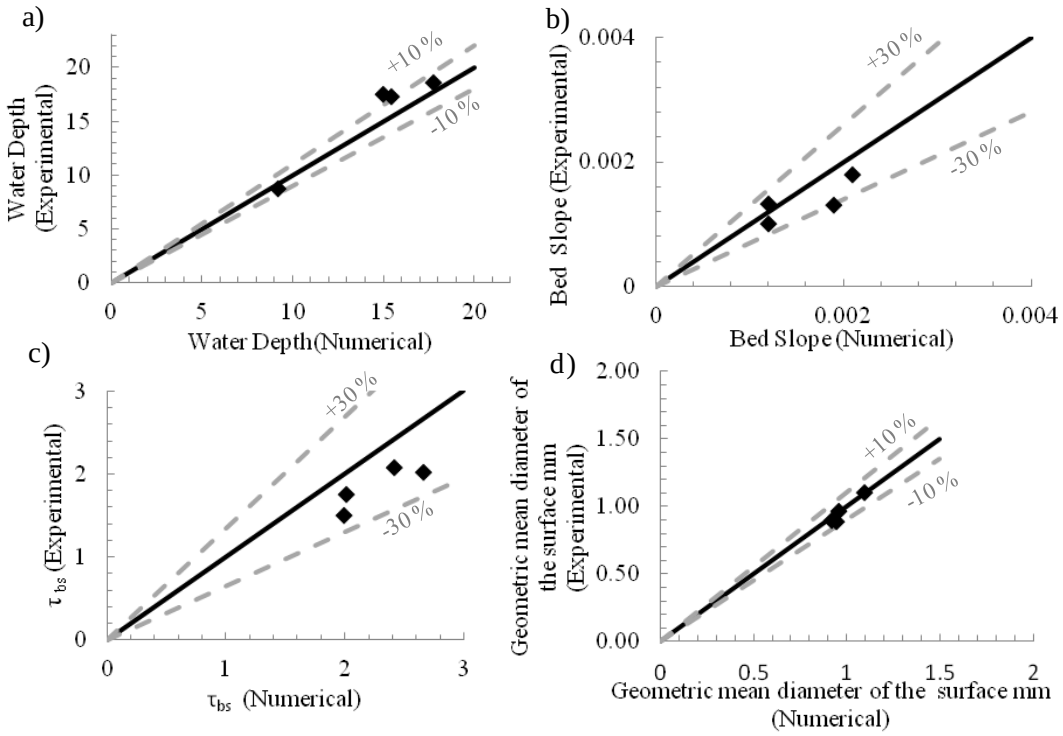

Figure 3.4 Comparison of flow and sediment characteristics of numerical and experimental results in fully alluvial cases. a) Water depth. b) bed slope. c) shear stress associated with skin friction. d) geometric mean diameter of the surface material.

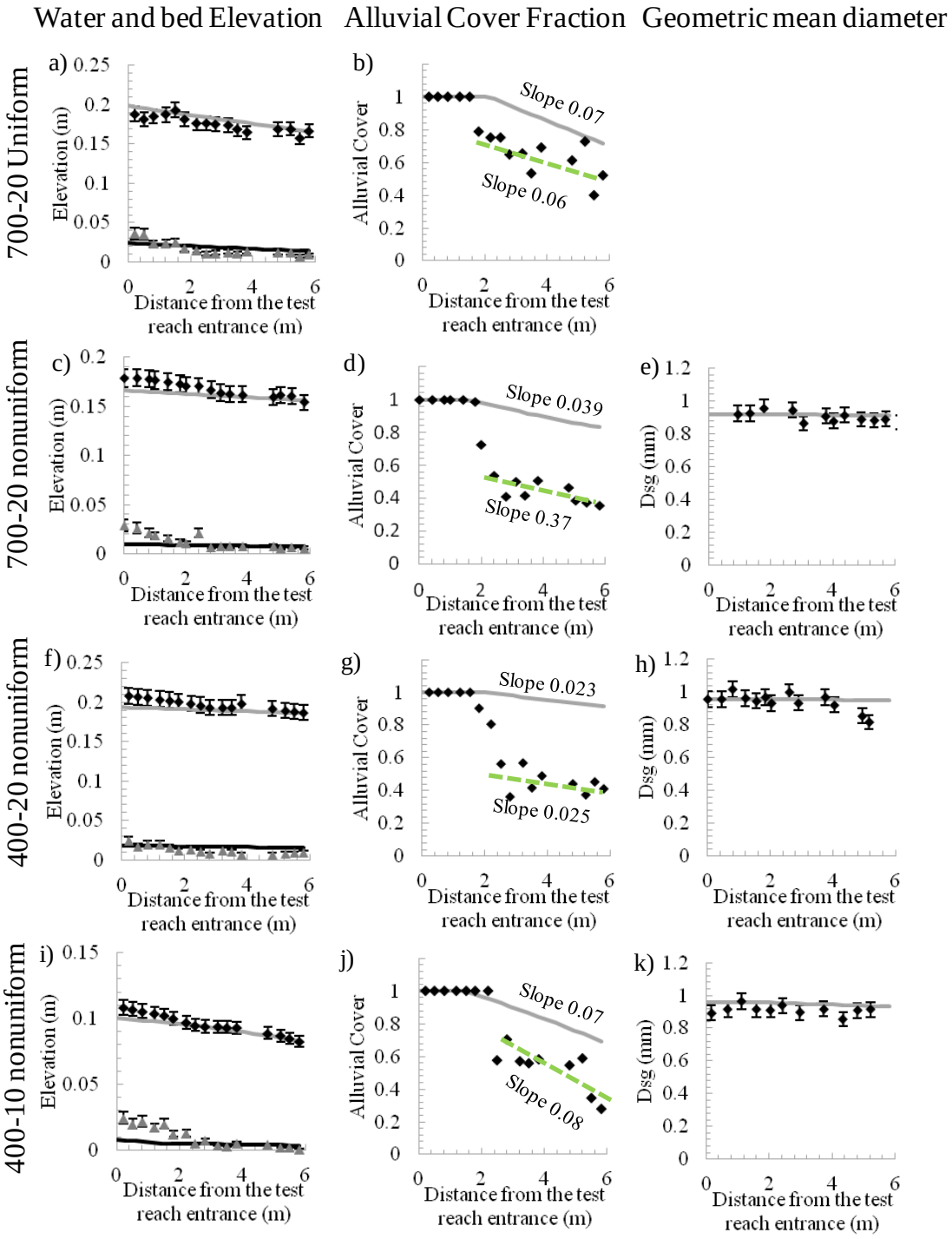

Figure 3.5 Water and bed surface elevation, sediment cover fraction and geometric mean diameter of the surface material for mixed bedrock-alluvial experiments (Runs 2, 4, 6 and 8 of chapter 2)

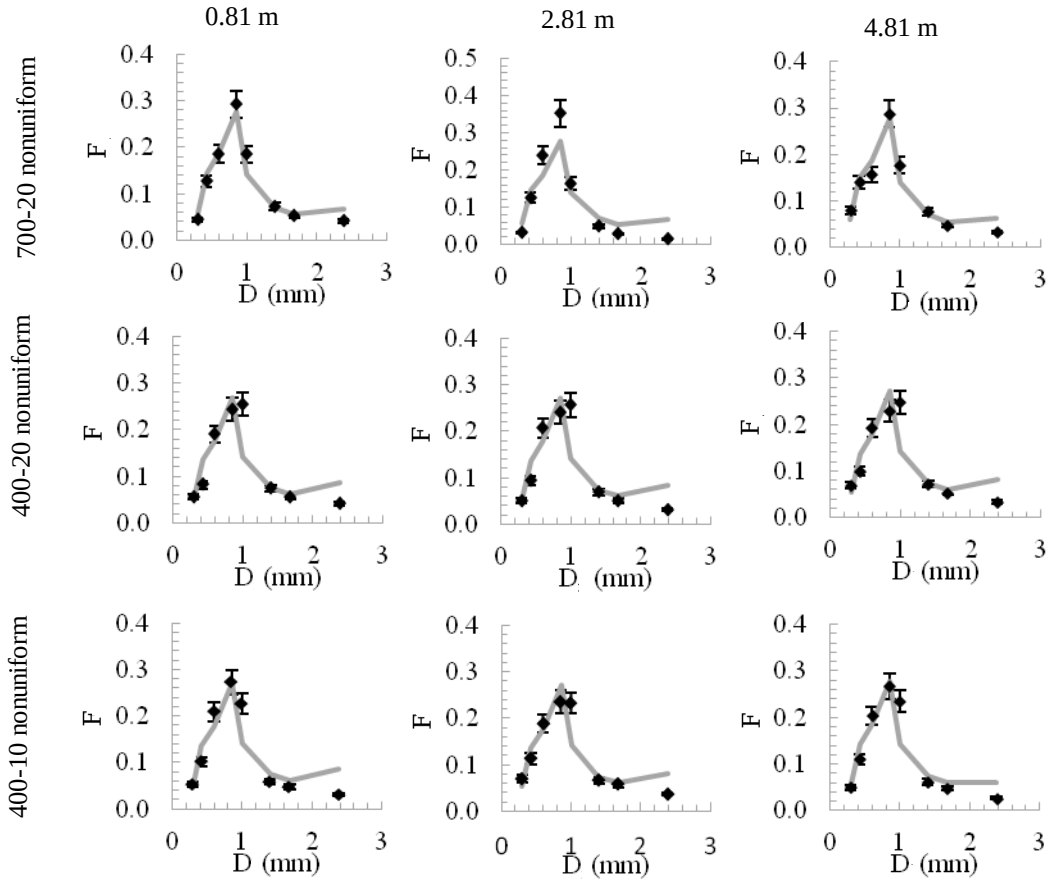

Figure 3.6 Grain size distribution of the surface material at upstream, middle and downstream of the test reach. Grey lines represent the numerical model and the diamonds denote the experimental data.

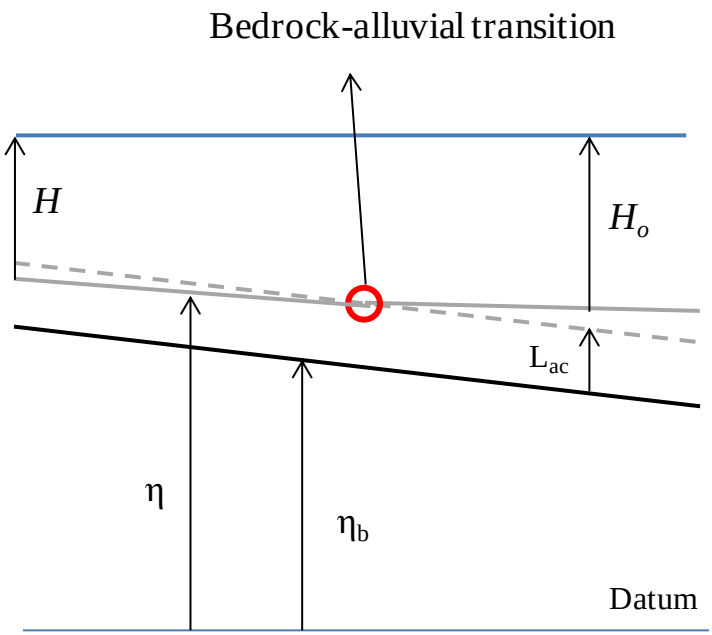

Figure 3.7 Schematic plot of a mixed bedrock-alluvial upstream of the bedrock-alluvial transition.

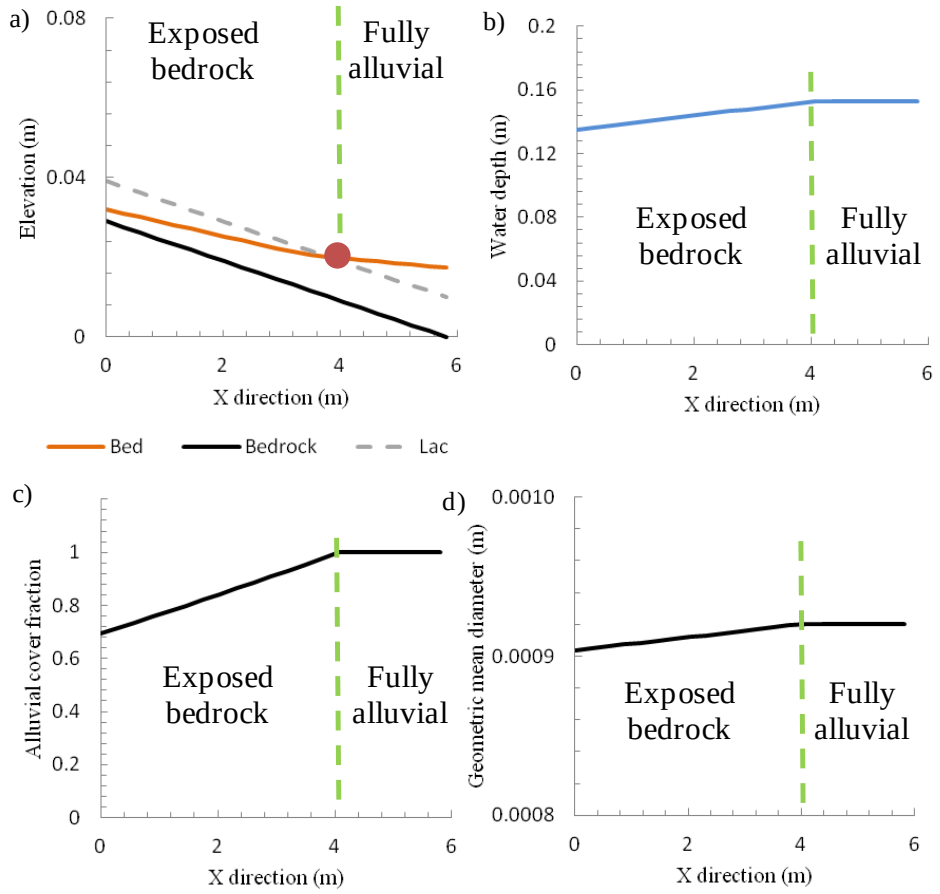

Figure 3.8 Bedrock-alluvial transition. a) bed surface (orange line), bedrock elevation (black line) and the minimum thickness of alluvial cover (dashed grey line). Red circle indicates the bedrock-alluvial transition. b) water depth. the green dashed lines represent the bedrock-alluvial transition. c) alluvial cover fraction. D) the geometric mean diameter of the surface sediment

CHAPTER 4

CONCLUSION

This dissertation presents laboratory experiments and mathematical modeling to investigate the alluvial morphodynamics of mixed bedrock-alluvial rivers transporting non-uniform bed material. Previous modeling studies of the alluvial morphodynamics of mixed bedrock-alluvial rivers demonstrated that, in the absence of subsidence, uplift and base level changes, mixed bedrock-alluvial reaches may reach a condition of equilibrium if bedrock incision is also neglected. Numerical simulations performed in the case of a constant friction coefficient and uniform sediment revealed that, based on the relative magnitude of the bedrock surface slope, S_b, and the alluvial equilibrium slope of a reach subject to the same flow regime and sediment supply, S_o, this equilibrium condition can either be characterized by a flow acceleration or by a flow deceleration over the mixed bedrock-alluvial reach.

Noting that bedform characteristics, grain size distribution of the bed surface material and sediment transport rate depend on the flow regime and the sediment supply, and that a perusal of the literature reveals that little is known about the alluvial morphodynamics of mixed bedrock-alluvial rivers, laboratory experiments were specifically designed to study the characteristics of the flow, of the bedload transport and of the bedforms in mixed bedrock-alluvial rivers. The experiments were performed in the

case of a “relatively mild”, bedrock surface, i.e. $S_b < S_o$, and the results were analyzed to study the spatial changes in flow resistances and bedload transport capacities of the flow.

The main results of the experimental study can be summarized as follows: when the bedrock surface slope is milder than the alluvial equilibrium slope of a reach subjected to the same flow regime and sediment supply the alluvial morphodynamics of a mixed bedrock-alluvial reach is characterized by

- Flow acceleration (Figure 2.6 panels b, d, g and j) in the streamwise direction due to the limited space to store sediment on the channel bed and to convey the flow. This spatial flow acceleration is associated with a decreasing alluvial cover in the direction of the flow;

- Changes in bedform height compared to the alluvial equilibrium case. In particular, in bedrock reaches the bedform height tends to be smaller than in the fully alluvial case and, due to the flow acceleration, it may decrease in the flow direction (Figure 2.6 panels a, c, f, i);

- Formation of a pattern of downstream fining of the bed surface sediment in response to the flow acceleration in the mixed bedrock-alluvial reach (Figure 2.6 panels e, h, k). Due to the increasing bed shear stress in the flow direction, and the system tends towards equal mobility conditions (unarmored surface) (Parker and Klinegman, 1982); The response of the bedforms and of the bed surface grain size to the presence of a non-erodible surface seems to be associated with the bedform regime (Figure 2.11). If the bedforms at equilibrium in a fully alluvial system subject to the flow regime and sediment

supply of the mixed bedrock-alluvial system are close to the dune-antidune transition (upper regime plane bed), a streamwise reduction in bedform height can be expected in the mixed bedrock-alluvial reach. If the equilibrium bedforms in a fully alluvial system with the same flow regime and sediment supply of the mixed bedrock-alluvial system are well in the dune regime, the formation of a stable pattern of downstream fining of the bed surface sediment can be expected in the mixed bedrock-alluvial reach.

The streamwise decrease in bedform height and/or bed surface grain size observed in the experiments results in a streamwise decrease in the flow resistances. This streamwise decrease of the flow resistances was associated with an increase of the bed material transport capacity in the mixed bedrock-alluvial reach, which balanced the streamwise reduction in alluvial cover fraction. The comparison between the experimental data on bedload transport and the grain size specific bedload transport rates estimated with the Ashida and Michiue (1972) bedload transport relation showed that surface-based formulations of bedload transport models were able to reasonably reproduce the grain size specific bedload transport rates in mixed bedrock-alluvial reaches, if the alluvial cover is used to balance the higher bedload transport capacities associated with the spatial flow acceleration.

The mathematical formulation to model the alluvial morphodynamics of mixed bedrock-alluvial rivers carrying non-uniform bed material was implemented in a one-dimensional numerical model and validated against the experimental data presented in Chapter 2. The validated model was used to characterize the flow hydrodynamics, the bedload transport and the sediment sorting patterns in mixed bedrock-alluvial rivers with

a bedrock slope steeper than S_o. This application revealed that at equilibrium when $S_b > S_o$ 1) the flow decelerates in the streamwise direction in the mixed bedrock-alluvial reach, 2) this spatial flow deceleration is associated with a streamwise decrease of the bed material transport capacity, thus 3) the alluvial cover increases in the streamwise direction to balance the reduction in the bed material transport capacity, and 4) a pattern of downstream coarsening characterizes the bed surface sediment to balance the spatial changes in relative mobility of coarse and fine sediment.

The proposed formulation for the alluvial morphodynamics of mixed bedrock-alluvial rivers has been validated at laboratory scale. The field scale validation will be performed on the lowermost ~30 kilometers of the Buech River in southeast of France. The validated model will be then applied to study the impacts of anthropogenic activities and restoration projects specifically designed to control in-channel sedimentation and improve the quality of the riparian habitat.

The Buech River is a braided gravel bed river in the western Alps in South East France that originates from the Massif du Dévoluy and joins the Durance River ~120 km downstream from its source just upstream of the town of Sisteron. Anthropogenic modification of the Buech River started in the 1800s with the construction of a system of levees and dikes that narrowed the braidplain. Gravel mining from the active channel started in the 1950s and ended in 2001, although minor gravel mining continued until 2012. In 1992 Saint Sauveur dam was closed on the Buech River to divert the flow (up to 30 m^3/s) to the Lazar power plant. After the closure of Saint Sauveur dam the coarse material is entirely trapped in the reservoir and changes in river morphology have been observed in the regulated reach of the Buech River. Field observations suggest that the gravel mining

and the closure of Saint Sauveur dam caused widespread erosion of the Buech River braidplain.

The closure of the St. Lazare dam on the Durance River few kilometers downstream of the Buech River – Durance River confluence further affected the flow hydrodynamics and the sediment transport regime in the lowermost part of the Buech River, which is now in the backwater zone of St. Lazare reservoir, with a consequent increase of the water levels and aggradation of the Buech River channel. In other words, the closure of St. Lazare dam represents a sudden raise in the water surface base level for the Buech River that induces channel bed aggradation towards equilibrium conditions that are enough to deliver the bed material load to the Durance River.

The response of the Buech River to the construction of the St. Lazare dam represents an increased flood risk for the city of Sisteron. In 2010 EDF, the French electric company operating St. Lazare dam, started a program of flood control characterized by sediment dredging in the lowermost 2 km of the Buech River braidplain to a depth of ~4 m. A total of ~800 m^3 of gravel was excavated from the braidplain. The amount of sediment accumulating in the dredged zone is evaluated biannually with two surveys, a winter survey (typically in January) to evaluate the amount of sediment accumulating in the dredged area and to decide if the zone needs to be dredged in the following summer. The summer survey is then performed to determine the volume of sediment that needs to be dredged during the summer low flow (typically in August).

The quantification of the impacts of the dredged zone on the morphology of the Buech River upstream from the backwater zone of the St. Lazare dam and the prediction

of the frequency of dredging operations are still a matter of debate. Sediment dredging in the lowermost 2 km of the Buech River can be described as the creation volumes to be filled with sediment to reduce channel bed aggradation in the upstream part of the system. However, research is needed to predict the long term (several decades) impact of the dredging on the Buech River upstream of the dredged zone.

In summary, the anthropogenic impacts on the Buech River between Saint Sauveur dam and the confluence with St. Lazare dam resulted in a significant reduction of the gravel supply, which is thought to have generated widespread erosion of the braidplain, and an increase in the downstream relative base level which induced in-channel sediment deposition.

The morphodynamics formulation presented in Chapter 3 and validated at field scale using the available information to characterize the undisturbed Buech River conditions will be used to 1) determine the long term evolution of the regulated Buech River, 2) assess if the long term evolution of the Buech River will result in increasing flood risk in the areas surrounding the Buech-Durance confluence, and 3) help EDF to design the dredging of the gravel pit upstream of the Buech-Durance confluence. Finally, the mathematical formulation presented in Chapter 3 of this dissertation will constitute the foundational piece for future model development to assess the long-term impacts of river restoration projects on the Buech River morphodynamics, on the aquatic and riparian habitat.

REFERENCES

Anderson, A. G., Parker, G., & Wood, A. (1975). The flow and stability characteristics of alluvial river channels.

Blom, A., Parker, G., Ribberink, J. S., & De Vriend, H. J. (2006). Vertical sorting and the morphodynamics of bed-form-dominated rivers: An equilibrium sorting model. *Journal of Geophysical Research: Earth Surface*, *111*(F1).

Blom, A., Viparelli, E., & Chavarrías, V. (2016). The graded alluvial river: Profile concavity and downstream fining. *Geophysical Research Letters*, 43(12), 6285-6293. doi: 10.1002/2016GL068898

Carling, P. A., Golz, E., Orr, H. G., & Radecki-Pawlik, A. (2000a). The morphodynamics of fluvial sand dunes in the River Rhine, near Mainz, Germany. I. Sedimentology and morphology. *Sedimentology*, *47*(1), 227-252. doi: 10.1046/j.1365-3091.2000.00290.x

Carling, P. A., Williams, J. J., Golz, E., & Kelsey, A. D. (2000b). The morphodynamics of fluvial sand dunes in the River Rhine, near Mainz, Germany. II. Hydrodynamics and sediment transport. *Sedimentology*, *47*(1), 253. doi: 10.1046/j.1365-3091.2000.00291.x

Chatanantavet, P., & Parker, G. (2008). Experimental study of bedrock channel alluviation under varied sediment supply and hydraulic conditions. *Water Resources Research*, *44*(12). doi: 10.1029/2007WR006581

Chatanantavet, P., & Parker, G. (2009). Physically based modeling of bedrock incision by abrasion, plucking, and macroabrasion. *Journal of Geophysical Research: Earth Surface*, *114*(F4). doi: 10.1029/2008JF001044

Chatanantavet, P., Whipple, K. X., Adams, M. A., & Lamb, M. P. (2013). Experimental study on coarse grain saltation dynamics in bedrock channels. *Journal of Geophysical Research: Earth Surface*, *118*(2), 1161-1176. doi: 10.1002/jgrf.20053

Chaudhry, M. H. (2007). *Open-channel flow*. Springer Science & Business Media.

Chiew, Y. M., & Parker, G. (1994). Incipient sediment motion on non-horizontal slopes. *Journal of Hydraulic Research*, *32*(5), 649-660.

Engelund, F., & Hansen, E. (1967). *A monograph on sediment transport in alluvial streams*. TEKNISKFORLAG Skelbrekgade 4 Copenhagen V, Denmark.

Fernandez Luque, R., & Van Beek, R. (1976). Erosion and transport of bed-load sediment. *Journal of hydraulic research*, 14(2), 127-144. doi: 10.1080/00221687609499677

Finnegan, N. J., Sklar, L. S., & Fuller, T. K. (2007). Interplay of sediment supply, river incision, and channel morphology revealed by the transient evolution of an experimental bedrock channel. *Journal of Geophysical Research: Earth Surface*, 112(F3). doi: 10.1029/2006JF000569

Garcia, M. H. (2008). Sediment transport and morphodynamics. In Sedimentation engineering: *Processes, measurements, modeling, and practice* (pp. 21-163). doi: 10.1061/9780784408148.ch02

Gasparini, N. M., Whipple, K. X., & Bras, R. L. (2007). Predictions of steady state and transient landscape morphology using sediment-flux-dependent river incision models. *Journal of Geophysical Research: Earth Surface*,*112*(F3). doi: 10.1029/2006JF000567

Hirano, M. (1971, November). River-bed degradation with armoring. In *Proceedings of the Japan Society of Civil Engineers* (Vol. 1971, No. 195, pp. 55-65). Japan Society of Civil Engineers.

Hodge, R. A., Hoey, T. B., & Sklar, L. S. (2011). Bed load transport in bedrock rivers: The role of sediment cover in grain entrainment, translation, and deposition. *Journal of Geophysical Research: Earth Surface*, *116*(F4). doi: 10.1029/2011JF002032

Hodge, R., Hoey, T., Maniatis, G., & Leprêtre, E. (2016). Formation and erosion of sediment cover in an experimental bedrock-alluvial channel. *Earth Surface Processes and Landforms*. doi: 10.1002/esp.3924

Howard, A. D. (1998). Long profile development of bedrock channels: Interaction of weathering, mass wasting, bed erosion, and sediment transport. *Rivers over rock: Fluvial processes in bedrock channels*, 297-319.

Inoue, T., Izumi, N., Shimizu, Y., & Parker, G. (2014). Interaction among alluvial cover, bed roughness, and incision rate in purely bedrock and alluvial-bedrock

channel. *Journal of Geophysical Research: Earth Surface*,*119*(10), 2123-2146. doi: 10.1002/2014JF003133

Johnson, J. P. (2014). A surface roughness model for predicting alluvial cover and bed load transport rate in bedrock channels. *Journal of Geophysical Research: Earth Surface*, *119*(10), 2147-2173. doi: 10.1002/ 2013JF003000.

Johnson, J. P., & Whipple, K. X. (2007). Feedbacks between erosion and sediment transport in experimental bedrock channels. *Earth Surface Processes and Landforms: The Journal of the British Geomorphological Research Group*, *32*(7), 1048-1062. doi : 10.1002/esp.1471

Lague, D. (2010). Reduction of long-term bedrock incision efficiency by short-term alluvial cover intermittency. *Journal of Geophysical Research: Earth Surface*, *115*(F2). doi: 10.1029/2008JF001210

Lague, D. (2014). The stream power river incision model: evidence, theory and beyond. *Earth Surface Processes and Landforms*, *39*(1), 38-61. doi: 10.1002/esp.3462

Lamb, M. P., Dietrich, W. E., & Sklar, L. S. (2008). A model for fluvial bedrock incision by impacting suspended and bed load sediment. *Journal of Geophysical Research: Earth Surface*, *113*(F3). doi: 10.1029/2007JF000915

Lauer, J. W., Viparelli, E., & Piégay, H. (2016). Morphodynamics and sediment tracers in 1-D (MAST-1D): 1-D sediment transport that includes exchange with an off-channel sediment reservoir. *Advances in Water Resources*, *93*, 135-149.

Nelson, P. A., & Seminara, G. (2012). A theoretical framework for the morphodynamics of bedrock channels. *Geophysical Research Letters*, *39*(6).

Nittrouer, J. A., Mohrig, D., Allison, M. A., & Peyret, A. P. B. (2011). The lowermost Mississippi River: a mixed bedrock-alluvial channel *Sedimentology*, *58*(7), 1914-1934. doi: 10.1111/j.1365-3091.2011.01245.x

Paola, C., Parker, G., Seal, R., Sinha, S. K., Southard, J. B., & Wilcock, P. R. (1992). Downstream fining by selective deposition in a laboratory flume. *SCIENCE-NEW YORK THEN WASHINGTON-*, *258*, 1757-1757.

Parker, G. (1990). Surface-based bedload transport relation for gravel rivers. *Journal of hydraulic research*, 28(4), 417-436. doi: 10.1080/00221689009499058

Parker, G. (1991). Selective sorting and abrasion of river gravel. I: Theory. *Journal of Hydraulic Engineering*, *117*(2), 131-147.

Parker, G. (1991). Selective sorting and abrasion of river gravel. II: Applications. *Journal of Hydraulic Engineering*, *117*(2), 150-171. doi: http://dx.doi.org/10.1061/(ASCE)0733-9429(1991)117:2(150)

Parker, G. (2008). Transport of gravel and sediment mixtures. *Sedimentation engineering: Processes, measurements, modeling, and practice*, *110*, 165-252. doi: 10.1061/9780784408148.ch03.

Parker, G. and Klingeman, P.C. (1982), On why gravel bed streams are paved, *Water Resources Research*, 18 (5), 1409–1433, 1982.

Parker, G., & Wilcock, P. R. (1993). Sediment feed and recirculating flumes: Fundamental difference. *Journal of Hydraulic Engineering*, 119(11), 1192-1204. doi: 10.1061/(ASCE)0733-9429.

Parker, G., Paola, C., & Leclair, S. (2000). Probabilistic Exner sediment continuity equation for mixtures with no active layer. *Journal of Hydraulic Engineering*, *126*(11), 818-826. doi: 10.1061/(ASCE)0733-9429.

Shaw, J. B., & Mohrig, D. (2014). The importance of erosion in distributary channel network growth, Wax Lake Delta, Louisiana, USA. *Geology*, *42*(1), 31-34.

Shaw, J. B., Mohrig, D., & Whitman, S. K. (2013). The morphology and evolution of channels on the Wax Lake Delta, Louisiana, USA. *Journal of Geophysical Research: Earth Surface*, *118*(3), 1562-1584. doi: 10.1002/jgrf.20123.

Sklar, L. S., & Dietrich, W. E. (2004). A mechanistic model for river incision into bedrock by saltating bed load. *Water Resources Research*, *40*(6). doi: 10.1029/2003WR002496

Tuijnder, A. P., Ribberink, J. S., & Hulscher, S. J. (2009). An experimental study into the geometry of supply-limited dunes. *Sedimentology*, *56*(6), 1713-1727. doi: 10.1111/j.1365-3091.2009.01054.x

Turowski, J. M., Lague, D., & Hovius, N. (2007). Cover effect in bedrock abrasion: A new derivation and its implications for the modeling of bedrock channel morphology. *Journal of Geophysical Research: Earth Surface*,*112*(F4). doi: 10.1029/2006JF000697

Van Rijn, L. C. (1984). Sediment transport, part III: bed forms and alluvial roughness. *Journal of hydraulic engineering*, 110(12), 1733-1754. doi: 10.1061/(ASCE)0733-9429(1984)110:12(1733)

Vanoni, V. A. (1975). Sedimentation Engineering*: American Society of Civil Engineers, Manuals and Reports on Engineering Practice*, (54), 745.

Vanoni, V. A., & Brooks, N. H. (1957). Laboratory studies of the roughness and suspended load of alluvial streams. Sedimentation Laboratory California Institute of Technology, Pasadena, California, Report No. E-68.

Viparelli, E., Gaeuman, D., Wilcock, P., & Parker, G. (2011). A model to predict the evolution of a gravel bed river under an imposed cyclic hydrograph and its application to the Trinity River. *Water Resources Research*, *47*(2). doi: 10.1029/2010WR009164

Viparelli, E., Haydel, R., Salvaro, M., Wilcock, P. R., & Parker, G. (2010). River morphodynamics with creation/consumption of grain size stratigraphy 1: laboratory experiments. Journal of Hydraulic Research, 48(6), 715-726. doi: 10.1080/00221686.2010.515383Viparelli, E., Gaeuman, D., Wilcock, P., & Parker, G. (2011). A model to predict the evolution of a gravel bed river under an imposed cyclic hydrograph and its application to the Trinity River. *Water Resources Research*, *47*(2). doi: 10.1029/2010WR009164

Viparelli, E., Lauer, J. W., Belmont, P., & Parker, G. (2013). A numerical model to develop long-term sediment budgets using isotopic sediment fingerprints. *Computers & geosciences*, 53, 114-122. doi:10.1016/j.cageo.2011.10.003

Viparelli, E., Nittrouer, J. A., & Parker, G. (2015). Modeling flow and sediment transport dynamics in the lowermost Mississippi River, Louisiana, USA, with an upstream alluvial-bedrock transition and a downstream bedrock-alluvial transition: Implications for land building using engineered diversions. *Journal of Geophysical Research: Earth Surface*, *120*(3), 534-563. doi: 10.1002/2014JF003257.

Viparelli, E., Sequeiros, O. E., Cantelli, A., Wilcock, P. R., & Parker, G. (2010). River morphodynamics with creation/consumption of grain size stratigraphy 2: Numerical model. *Journal of Hydraulic Research*, *48*(6), 727-741.

Whipple, K. X. (2004). Bedrock rivers and the geomorphology of active orogens. *Annu. Rev. Earth Planet. Sci.*, *32*, 151-185. doi: 10.1146/annurev.earth.32.101802.120356

Whipple, K. X., & Tucker, G. E. (2002). Implications of sediment-flux-dependent river incision models for landscape evolution. *Journal of Geophysical Research: Solid Earth*, *107*(B2). doi: 10.1029/2000JB000044

Whipple, K. X., Hancock, G. S., & Anderson, R. S. (2000). River incision into bedrock: Mechanics and relative efficacy of plucking, abrasion, and cavitation. *Geological Society of America Bulletin*, *112*(3), 490-503. doi: 10.1130/0016-7606(2000)112

Wilcock, P. R., & Crowe, J. C. (2003). Surface-based transport model for mixed-size sediment. *Journal of Hydraulic Engineering*, 129(2), 120-128. doi: 10.1061/(ASCE)0733-9429(2003)129:2(120)

Wong, M., Parker, G., DeVries, P., Brown, T. M., & Burges, S. J. (2007). Experiments on dispersion of tracer stones under lower-regime plane-bed equilibrium bed load transport. *Water Resources Research*, *43*(3). doi: 10.1029/2006WR005172

Wright, S., & Parker, G. (2004). Flow resistance and suspended load in sand-bed rivers: simplified stratification model. *Journal of Hydraulic Engineering*, 130(8), 796-805. doi: 10.1061/(ASCE)0733-9429(2004)130:8(796)

Zhang, L., Parker, G., Stark, C. P., Inoue, T., Viparelli, E., Fu, X., & Izumi, N. (2015). Macro-roughness model of bedrock-alluvial river morphodynamics. *Earth Surface Dynamics Discussions*, *2*, 297-355. doi: 10.5194/esurfd-2-297-2014

APPENDIX A

PROCEDURES TO REMOVE SIDEWALL EFFECTS AND EINSTEIN DECOMPOSITION

Introduction

A.1 describes the procedure to remove the sidewall effects used to estimate the value of the shear stress acting on the bed [*Vanoni and Brooks*, 1957; *Chiew and Parker*, 1990]. A.2 illustrates the procedure to partition the flow resistances between skin friction and form drag i.e. the Einstein decomposition [*Parker*, 2004].

A.1 Procedure to remove the sidewall effects

To remove the effects of the smooth sidewalls and estimate the shear stress acting on the rough bed, we followed the procedure introduced by *Vanoni and Brooks* [1957] as outlined in *Chiew and Parker* [1994]. The main assumption is that the cross section can be divided into two non-interacting regions, the bed region and the wall region. It is further assumed that:

1) In wall and in the bed region the streamwise component of the gravity force is balanced by the shear stresses acting on the walls and, on the bed, respectively;

2) The mean flow velocity U and the energy gradient S_f are the same in the entire cross section, in the wall and in the bed region; and

3) The Darcy Weisbach resistance relation can be applied to each region and to the entire cross section.

Under these assumptions, the equations of mass and momentum conservation respectively reduce to

$$A_{cs} = A_w + A_b \tag{A-1}$$

$$C_{f,cs}P_{cs} = C_{f,w}P_w + C_{f,b}P_b \tag{A-2}$$

with *A* denoting the cross-sectional area, *P* the wetted perimeter, and C_f a non-dimensional friction coefficient equal to the Darcy-Weisbach friction factor *f* divided by 8. The subscripts *cs*, *w* and *b* respectively denote the entire cross section, the wall and the bed region. In the case of a rectangular cross section, the wetted perimeter of the bed region is equal to the section width and the wetted perimeter of the wall region is equal to *2H*, with *H* denoting the water depth.

The condition that the energy gradient for the entire cross section is equal to the energy gradient in the bed and in the wall region is expressed with the aid of the Darcy Weisbach relation as follows

$$\frac{C_{f,cs}U^2}{gr_{cs}} = \frac{C_{f,w}U^2}{gr_w} = \frac{C_{f,b}U^2}{gr_b} \tag{A-3}$$

where *g* denotes the acceleration of gravity and *r* is the hydraulic radius, equal to the cross-sectional area divided by the wetted perimeter. Equation (A-3) is simplified using the definition of Reynolds number $Re = rU/\nu$, with ν being kinematic viscosity of water:

$$\frac{C_{f,cs}}{Re_{cs}} = \frac{C_{f,w}}{Re_w} = \frac{C_{f,b}}{Re_b} \tag{A-4}$$

The unknowns in equations (A-1), (A-2) and (A-4) are $C_{f,b}$, $C_{f,w}$, A_b *and* A_w. Thus, a fourth equation is needed to solve the problem.

Noting that the flume sidewalls are smooth compared to the channel bed, which is covered with sediment, we use the Nikuradse relation for smooth pipes (equation A-5) to compute the friction coefficient of the bed region

$$\frac{1}{\sqrt{f_w}} = 0.86ln\left(4Re_w\sqrt{f_w}\right) - 0.8 \qquad \text{(A-5)}$$

Equations (A-1), (A-2), (A-4) and (A-5) are iteratively solved to compute the friction coefficient and the area of the bed and of the wall regions. The sidewall corrected friction coefficient, $C_{f,b}$, was used to compute the shear stress acting on the bed.

A.2 Partition of the flow resistances

When bedforms are present part of the drag is associated with the complex interactions between the flow and the bedforms (form drag) and does not contribute directly to bedload transport [*Parker*, 2004]. To perform sediment transport calculations, it is thus necessary to estimate the part of the drag acting tangentially to the channel bed (skin friction), which is thought to be responsible for moving the sediment in the flow direction.

The skin friction is computed considering an ideal flow over a flat bed with the same grain roughness, energy slope, S_f; and mean flow velocity, U, of the flow in the presence of bedforms. To compute the hydraulic radius, $r_{b,s}$ and the bed friction coefficient, $C_{f,bs}$, of this ideal flow, i.e. the values associated with skin friction, we used

1) a Manning-Strickler resistance formulation - equation (6) [*Parker*, 1991],

2) the product of the hydraulic radius and the energy slope to compute the bed shear stress – equations (7a) and (7b) [*Chiew and Parker*, 1994], and

3) the product of the non-dimensional friction coefficient and of the mean velocity squared to compute the bed shear stress – equations (8a) and (8b) [*Vanoni*, 1975].

The system of equations to compute $r_{b,s}$ and $C_{f,bs}$ takes the form

$$C_{f,bs}^{-0.5} = \alpha_r \left(\frac{r_{b,s}}{k_s}\right)^{\frac{1}{6}} \tag{A-6}$$

$$\tau_b = \rho R r_b S_f \qquad \tau_{b,s} = \rho R r_{b,s} S_f \tag{A-7a, b}$$

$$\tau_b = \rho C_{f,b} U^2 \qquad \tau_{b,s} = \rho C_{f,bs} U^2 \tag{A-8a, b}$$

where α_r is a constant equal to 8.1 [*Parker*, 2004], k_s represents the roughness height, ρ is the water density, g the acceleration of gravity and the subscript s indicates values that are associated with skin friction.

Recalling that the energy slope and the mean flow velocity of the ideal flow considered herein are equal to the energy slope and the mean flow velocity of the flow in presence of bedforms, equations (A-7) and (A-8) are reduced to

$$\frac{C_{f,b}}{r_b} = \frac{C_{f,bs}}{r_{b,s}} \tag{A-9}$$

To compute $C_{f,bs}$ and $r_{b,s}$ with equations (A-6) and (A-9) the roughness height k_s has to be specified. We assume that the roughness height is a linear function of the diameter of the

bed surface sediment such that 90% of the sediment is finer, D_{s90}, i.e. $k_s = n_k D_{s90}$, with $n_k = 2$ [*Parker*, 2004].